

Modification Strategies of High-Nickel Layered Oxide Cathode for Lithium-Ion Batteries

Mengxi Cai, Wen Yang, and Zhenguo Wu*

The rapid expansion of modern industry has resulted in an over-reliance on fossil fuels, leading to global energy crises and environmental issues. China has established “dual-carbon” goals to address these challenges, aiming to achieve carbon peaking by 2030 and carbon neutrality by 2060. Meeting these targets necessitates a transition from traditional fossil fuels to renewable energy sources and the development of low-cost, high-performance energy storage systems. Lithium-ion batteries, characterized by their low cost, high energy density, long life, and safety, have emerged as a key technology. High-nickel layered cathode materials, such as LiNiO_2 and $\text{LiNi}_{1-x-y}\text{Co}_x\text{Mn}_y\text{O}_2$ (NCM), offer higher

specific capacities and lower costs than traditional materials like LiCoO_2 . However, they face significant challenges, including cation mixing, oxygen evolution, transition metal ion dissolution, and structural instability during cycling. This review discusses various modification strategies, including innovative synthesis methods, element doping, surface coating, single-crystal design, and concentration gradient structures, to enhance the stability and performance of high-nickel cathodes. The study concludes that while high-nickel cathodes show promise, further research is needed to balance energy density, safety, and cost-effectiveness for large-scale commercial applications.

1. Introduction

With the rapid development of modern industry and science and technology, the traditional fossil fuels represented by oil, natural gas, and coal have been over-exploited and utilized, which has not only triggered the global energy crisis but also caused serious environmental pollution and climate change problems.^[1,2] To achieve better sustainable development, China has actively responded to global green and low-carbon development and put forward the “dual-carbon” development goals of “carbon peaking” and “carbon neutrality.” As a global energy-consuming country, China has a “coal-rich, oil-poor, gas-poor” energy structure, and it needs to import a large amount of natural gas and oil every year to meet the current demand. Therefore, it is urgent to adjust the energy structure and innovate technology to achieve the “dual carbon” goal, which is conducive to promoting green sustainable development and ensuring national energy security.

The key to achieving the “dual carbon” goal is to promote the development of new renewable energy sources and gradually reduce the dependence on traditional fossil fuels. Renewable energy, such as solar, wind, tidal, and geothermal energy, generally has the defects of unconcentrated regional distribution and difficult continuous supply. Considering that the operation of power grids requires a continuous and stable supply of electricity, it is difficult for the electricity provided by these renewable energy sources to meet the demand for stability of the grid. Therefore, the development and construction of low-cost energy storage systems have important research value to meet the needs

of green sources. Compared with flywheel energy storage and compressed air energy storage, electrochemical energy storage systems, typically represented by lithium-ion batteries, have comprehensive advantages of low cost, high energy density, long life, and high safety.^[3,4]

In recent years, with the rapid development of lithium-ion batteries, their applications have become no longer limited to energy storage, power tools, and portable consumer electronics. They have been widely used in many fields, such as military equipment and aerospace.^[5,6] Therefore, designing new battery structures and innovating battery materials are crucial to promoting the further development and application of lithium-ion batteries.

Lithium-ion batteries have evolved significantly since their inception. Lithium, discovered in 1817 by Arfvedson and Berzelius,^[7] has a low density ($\rho = 0.53 \text{ g cm}^{-3}$) and high specific capacity (3860 mAh g⁻¹), making it ideal for batteries. However, its reactivity limited early development until Harris found that lithium could be stabilized in nonprotonic solvents in 1958,^[8] leading to the commercialization of nonaqueous lithium primary batteries.

In 1972, Armand et al.^[9] introduced the concept of intercalation compounds through studies on ion-embedded Prussian blue materials, while Steele et al.^[10] showed that transition metal disulfide could serve as intercalation electrode materials. In 1974, Rao and Rouxel et al.^[9–11] also reported that metal chalcogenides exhibit faster intercalation kinetics. Whittingham^[12] then used layered transition metal disulfides to reversibly store lithium ions at room temperature via the “intercalation mechanism” (Figure 1). However, dendritic lithium deposition and safety issues hindered progress.

In 1979, Godshall et al.^[13] demonstrated the de-embedding properties of LiCoO_2 at high potentials and temperatures, followed by Goodenough’s 1980 report^[14] on its room-temperature

M. Cai, W. Yang, Z. Wu
School of Chemical Engineering
Sichuan University
Chengdu 610065, P. R. China
E-mail: zhenguowu@scu.edu.cn

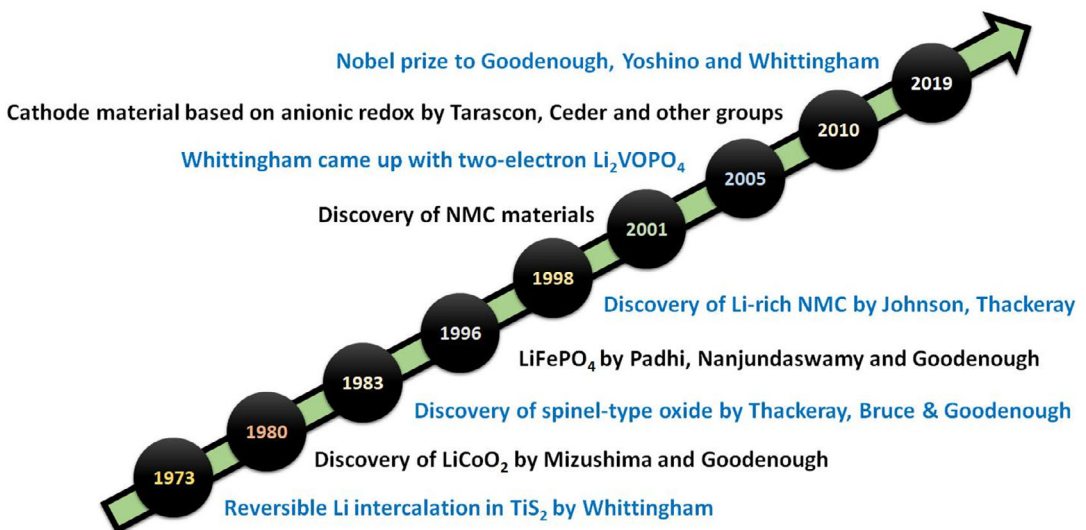


Figure 1. The progression of lithium-ion batteries reproduced with permission.^[9] Copyright 2021, LIDSEN Publishing Inc.

ion deembedding, advancing $LiCoO_2$ cathode development. Basu and Yazami's work^[15,16] on reversible lithium de-embedding in graphite laid the foundation for graphite anodes. Dahn et al.^[17] improved cycle performance by using ethylene carbonate to enhance solid electrolyte interface (SEI) formation and inhibit propylene carbonate decomposition.

Sony commercialized the first 18,650 lithium-ion battery in 1991 using $LiCoO_2$ and petroleum coke with a $LiPF_6$ -based electrolyte.^[18] In 1996, Goodenough et al.^[19] introduced $LiFePO_4$ as a cathode material, though its poor conductivity initially hindered application. Armand et al.^[9] later improved this through carbon coating. Layered oxide NCM cathodes gained attention for higher discharge capacities, and Thackeray et al.^[20] introduced lithium-rich NCM cathodes in 2005, enhancing conductivity and cycling stability with carbon coatings.

In 2019, the Nobel Prize in Chemistry was awarded to J.B. Goodenough, Akira Yoshino, and M.S. Whittingham for their pioneering contributions to lithium-ion battery technology.

Lithium-ion batteries mainly comprise cathode, anode, separators, electrolytes, and collectors. The reaction mechanism of lithium-ion batteries, which vary with electrode materials, can be classified into eight types (as shown in Figure 2). Among them, the reversible de-embedding reaction (e.g., $LiCoO_2$), phase change reaction (e.g., $LiFePO_4$), and transformation reaction (e.g., MnO , FeF_3) are the most widely studied mechanisms.^[21] Other mechanisms, such as reversible chemical bonding, organic oxygen radical reactions, and surface/interface charge storage, are still in the basic research stage.

The basic working principle inside the lithium battery is shown in Figure 3, using a battery with $LiCoO_2$ as the cathode and graphite as the anode. When charging, Li^+ is removed from the $LiCoO_2$ lattice (Equation (1)), solvates with electrolyte molecules, migrates through the separators to the anode, and then intercalates into the graphite anode (Equation (2)). Electrons move from the cathode to the anode via the external circuit, while Co^{3+} is oxidized to Co^{4+} to maintain charge balance. During discharge, electrons flow from the anode to the cathode,



Mengxi Cai is currently an undergraduate student in the School of Chemical Engineering at Sichuan University. Her research focuses on the cathode material of LiBs.



Wen Yang obtained his Ph.D. (2023) from Sichuan University with Prof. Ben-He Zhong. His research focuses on the cathode material of LiBs.



Zhenguo Wu obtained his Ph.D. (2016) from Sichuan University with Prof. Ben-He Zhong. He is currently an associate researcher at Sichuan University. His research interests include the development of advanced energy materials for lithium-ion and sodium-ion batteries.

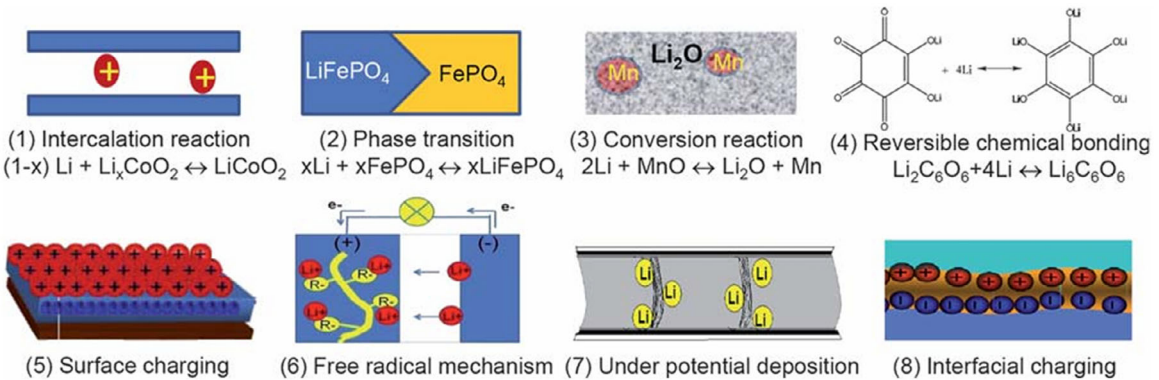


Figure 2. The schematic illustration of reversible lithium storage mechanism for lithium-ion batteries. Reproduced with permission.^[21] Copyright 2011, RSC publishing.

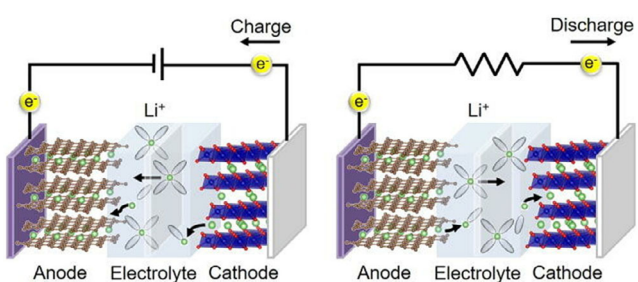


Figure 3. The schematic representation of the working mechanism for lithium-ion batteries. Reproduced with permission.^[165] Copyright 2022, AIP publishing.

and Li^+ de-intercalates from graphite and re-enters the $\text{Li}_{1-x}\text{CoO}_2$ lattice. The whole chemical reaction process is summarized as follows

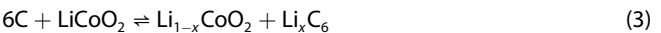
cathodic process:



anodic process:



total battery reaction:



2. Cathode Materials for Lithium-Ion Batteries

The current cathode materials for lithium-ion batteries can be mainly divided into the following four categories:^[22] 1) layered transition metal oxide cathode (Figure 4a), such as LiNiO_2 and $\text{LiNi}_x\text{Co}_y\text{Mn}_z\text{O}_2$, etc.; 2) olivine-structured cathode (Figure 4c), such as LiFePO_4 and $\text{Li}_3\text{V}_2(\text{PO}_4)_3$, etc.; 3) spinel-structured cathode (Figure 4d), such as LiMn_2O_4 etc.; and 4) disordered rock salt structure cathode (Figure 4e), such as $\text{Li}_{1.2}\text{Mn}_{0.4}\text{Ti}_{0.4}\text{O}_2$, etc. The above four types of cathode materials are discussed in detail below.

2.1. Layered Structure Cathode Material

The layered structure cathode material LiMO_2 (M for Ni, Mn, Co, etc.) is an $\alpha\text{-NaFeO}_2$ structure with a spatial point group of R-3m. The crystal structure is shown in Figure 4b, with oxygen in LiMO_2 (R-3m) forming a face-centered cubic lattice, transition metal, and Li occupying octahedral positions. The oxygen planes are

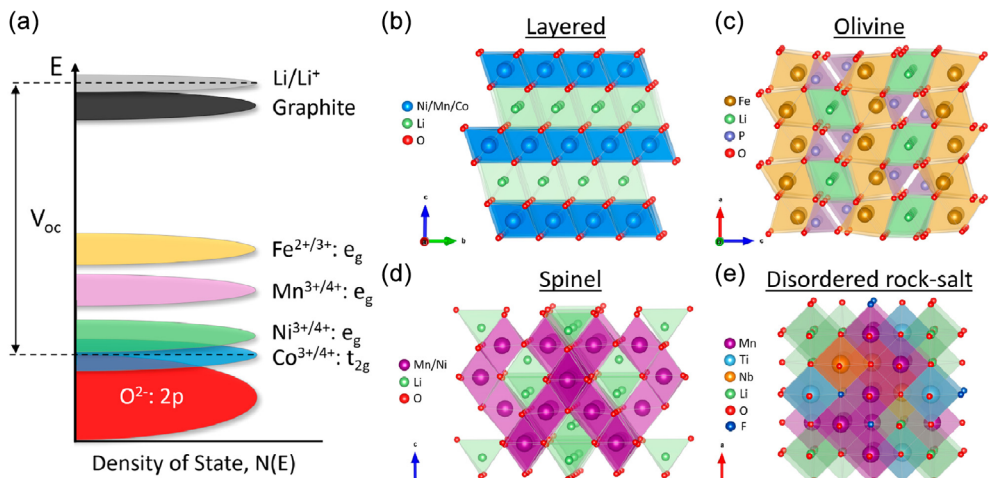


Figure 4. a) Redox energies of Co, Ni, Mn and Fe relative to Li/graphite; The crystal structures schematic of the b) layered oxides $\text{LiNi}_x\text{Mn}_y\text{Co}_z\text{O}_2$, c) olivine LiFePO_4 , d) spinel $\text{LiNi}_x\text{Mn}_y\text{O}_4$, and e) disordered rock salt $\text{Li}_2\text{Mn}_x\text{Nb}_y\text{Ti}_z\text{O}_{3-z}\text{F}_z$. Reproduced with permission.^[166] Copyright 2022, ACS publishing.

alternately stacked in ABCABC order, which is called the layered O₃ structure. Lithium ions move within the structure through a 2D diffusion pathway within the lithium layer, and the transport mechanism can be categorized into ODH (oxygen dumbbell hopping) and TSH (tetrahedral site hopping).^[22] At the initial stage of charging, lithium-ion transport is mainly based on the ODH mechanism, that is, lithium-ion migrates from one octahedral position to the adjacent octahedral position through the adjacent oxygen position. As the amount of lithium in the structure decreases, lithium ions migrate from one octahedral position to the next through the middle tetrahedral position (TSH mechanism). The layered structure cathode materials that are widely studied at present mainly include LiCoO₂, LiNiO₂, LiNi_{1-x-y}Co_xMn_yO₂, LiNi_{1-x-y}Co_xAl_yO₂, and lithium-rich manganese-based materials.

LiCoO₂ is the first commercial application of layered structure cathode material and also the most mature cathode material so far; its main advantages are as follows. 1) High energy density. Its theoretical specific capacity is up to 273 mAh g⁻¹, its theoretical density is about 5.06 g cm⁻³, and its compacted density is 4.0–4.2 g cm⁻³.^[23] However, when the LiCoO₂ cut-off voltage is 4.2 V, only about half of the lithium is removed from the structure, and the specific discharge capacity of the material is only 160 mAh g⁻¹.^[23] When the cut-off voltage is increased to 4.45 V, LiCoO₂ can provide a capacity of about 175 mAh g⁻¹ and a volume-specific energy of more than 2900 Wh L⁻¹, which is far better than that of materials such as commercial LiFePO₄. 2) Excellent structural stability, high electrical conductivity, and lithium-ion diffusion coefficient. On the one hand, due to the large difference in charge and ionic radius between Li⁺ and Co³⁺ ions, there is good cation ordering, promoting lithium ions' 2D fast diffusion. On the other hand, the direct interaction between Co–Co atoms also contributes to improving electronic conductivity.^[24] In addition, due to the occurrence of holes in the Co^{3+/4+}: t_{2g}^{6-x} band with low spin, which leads to the overlap of valence and conduction bands, Li_{1-x}CoO₂ transforms into metallization, and the electronic conductivity is significantly enhanced.^[25,26]

The current research on LiCoO₂ mainly focuses on the development of its high voltage (4.5–4.7 V) performance to achieve the purpose of improving energy density. However, the development of high-voltage lithium cobaltate faces many problems. On the one hand, since the low-spin Co^{3+/4+} band overlaps with the top of the O²⁻: 2p band (as shown in Figure 5), when the amount of lithium extracted from Li_{1-x}CoO₂ exceeds 50%, the oxygen ions in the lattice will be involved in the charge compensation

resulting in the oxygen precipitation, which not only increases the gas production of the battery but also destroys the intrinsic structure.^[27] On the other hand, during the removal of lithium ions from LiCoO₂, the oxygen layer will rearrange and form a cubic close-packed oxygen lattice with different degrees of distortion, so the structure will undergo a series of O₃ → H1-3 → O₁ phase transitions.^[28,29] The phase transition produces a huge lattice dislocation, accompanied by a drastic contraction of the lattice constant *c*, which causes the accumulation of nonuniform stress within the particles and eventually leads to the formation of microcracks or even the fragmentation of the particles and the volumetric expansion of the core.^[30] In addition, the high valence Co⁴⁺ has a strong catalytic activity, so it will exacerbate the decomposition of the electrolyte, which will cause severe gas production and Co dissolution. The decomposition products then increase internal resistance and polarization, further exacerbating the performance degradation of LiCoO₂ at high voltage. Finally, due to the poor thermal stability of LiCoO₂, a large amount of oxygen is released from the positive electrode once the temperature exceeds a critical value, resulting in severe thermal runaway.^[31] Usually, when the temperature exceeds 200 °C, LiCoO₂ batteries have a greater risk of thermal runaway. And cobalt is not only expensive but also toxic.^[32] Therefore, the current LiCoO₂ cathode is only widely used in the field of consumer electronics, failing to occupy the energy storage and power battery market.

The crystal structures of LiNiO₂ and LiCoO₂ are similar, but LiNiO₂ has a higher reversible specific capacity (>200 mAh g⁻¹), which may be related to the different electronic structures between Co and Ni.^[33] As shown in Figure 5, the crystal field formed by octahedral oxygen anion coordination divides the five transition metal d-orbitals into two sets of energy levels, e.g., and t_{2g}. Among them, the e_g level is more likely to lose electrons and occupies a higher position on the energy band diagram.^[30] Therefore, during charging, the electronic structure of Co³⁺ with six d-band electrons shifts from t_{2g}⁶ to t_{2g}⁵. In contrast, the oxidation of Ni³⁺ with seven d-band electrons shifts from t_{2g}⁶e_g¹ to t_{2g}⁶, which means that Co³⁺ has higher oxidation barriers than Ni³⁺ and because the region of overlap of the t_{2g} with the O²⁻: 2p energy band is relatively higher in Co^{3+/4+} compared to Ni^{3+/4+}, Ni^{3+/4+} has relatively fewer electronic domains and thus can release a higher reversible specific capacity.^[33] However, the low-spin Ni³⁺ tends to have a long octahedral NiO₆ ligand due to the Jahn-Teller effect, while the corresponding NiO₆ of Ni⁴⁺ has an ortho-octahedral geometry.^[23] Therefore, the oxidation process of Ni³⁺ in LiNiO₂ is unavoidably accompanied by structural distortions that cause structural transformations.^[30] In addition, the calcination process leads to the formation of part of Ni²⁺(0.69 Å), which has an ionic radius similar to that of Li⁺(0.76 Å), thus causing the migration of Ni²⁺ to the lithium layer, resulting in a severe Li⁺/Ni²⁺ mixing and discharging phenomenon. Moreover, LiNiO₂ is more sensitive to humidity. It thus is highly susceptible to reacting with H₂O and CO₂ in the air and generating surface residual lithium consisting of LiOH and Li₂CO₃, which exacerbates the performance degradation and cell gas production.^[34] In addition, Ni⁴⁺ with strong oxidizing properties is highly susceptible to severe interfacial side reactions with

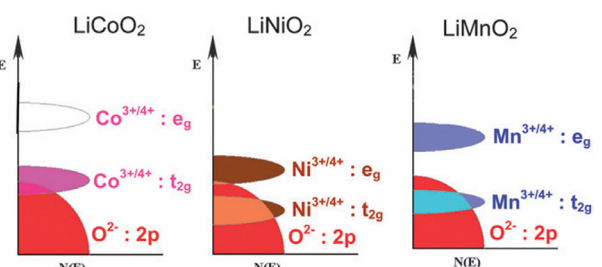


Figure 5. The electronic band structure of LiCoO₂, LiNiO₂ and LiMnO₂. Reproduced with permission.^[33] Copyright 2008, RSC publishing.

the electrolyte in the high charge state, thus exacerbating the structural instability.^[35] All these bottlenecks have hindered the commercial application of LiNiO₂.^[35]

For the layered LiMnO₂ cathode material, compared with the raw material cost of Co and Ni, Mn is cheaper and less toxic. LiMnO₂ has a high capacity of about 285 mAh g⁻¹ and a higher power density. Moreover, Mn ions possess excellent thermodynamic stability because the Mn^{3+/4+}: e.g., energy band is significantly higher than the O²⁻: 2p energy band.^[30] However, the MnO₆ octahedron is prone to distortion due to the Jahn-Teller effect, resulting in a less symmetrical orthorhombic system. On the other hand, Mn³⁺ is prone to disproportionation reactions leading to the formation of Mn²⁺ and Mn⁴⁺.^[36] And the formed Mn²⁺ has high solubility, which results in severe Mn leaching. The dissolved Mn ions migrate to the negative electrode, damage the negative electrode's SEI membrane, increase the impedance, and exacerbate the performance degradation.^[37] Therefore, the poor cycling stability of LiMnO₂ hinders its widespread commercialization.

In order to balance the cost, specific capacity, cycle stability, and safety performance, Li_{1-x-y}Co_xMn_yO₂ (NCM) has gradually become a mainstream cathode material. As shown in Figure 6, each transition metal ion in NCM has its own advantages and disadvantages. For Mn, the e.g., energy band of Mn^{3+/4+} is significantly higher than the t_{2g} energy band of Co^{3+/4+} and the e.g., energy band of Ni^{3+/4+}.^[30] Therefore, during the charging process, Mn maintains the +4 valence all the time and does not

participate in the electrochemical redox reaction, thus enhancing the stability of the structure. However, due to the small octahedral stabilization energy of Mn, it is highly susceptible to migrate from the octahedral sites of the TM layer to the octahedral sites of the Li layer through the neighboring tetrahedral sites, triggering the transformation of the layered structure into a spinel structure with concomitant voltage decay. In contrast, Co has excellent structural stability and large octahedral stabilization energy, which can enhance the structural stability of NCM.^[38] As for Ni, the Ni^{3+/4+} energy bands basically do not touch the top of the O²⁻: 2p band, and thus Ni³⁺ can be oxidized to Ni⁴⁺, which not only provides more capacity but also does not eliminate the electron density of the O²⁻: 2p band as well as cause oxygen precipitation from the lattice.^[38,39] In addition, Ni³⁺ has a structural stability of octahedral stabilization energy between that of Mn³⁺ and Co³⁺. Therefore, developing high-Ni ternary cathode materials with high specific capacity has become a hotspot for current scientific research and commercial applications, which will be further detailed in the following.

In addition to the conventional layered cathode materials mentioned above, there is a class of lithium-rich layered oxide xLi₂MnO₃·(1-x)LiTMO₂ in the form of lithium excess, which has attracted much attention from researchers due to its lower cost and reversible specific capacity of more than 250 mAh g⁻¹. The crystallographic structure of Li-rich layered oxides can be represented by 1) monoclinic Li₂MnO₃ (C2/m) coexisting with

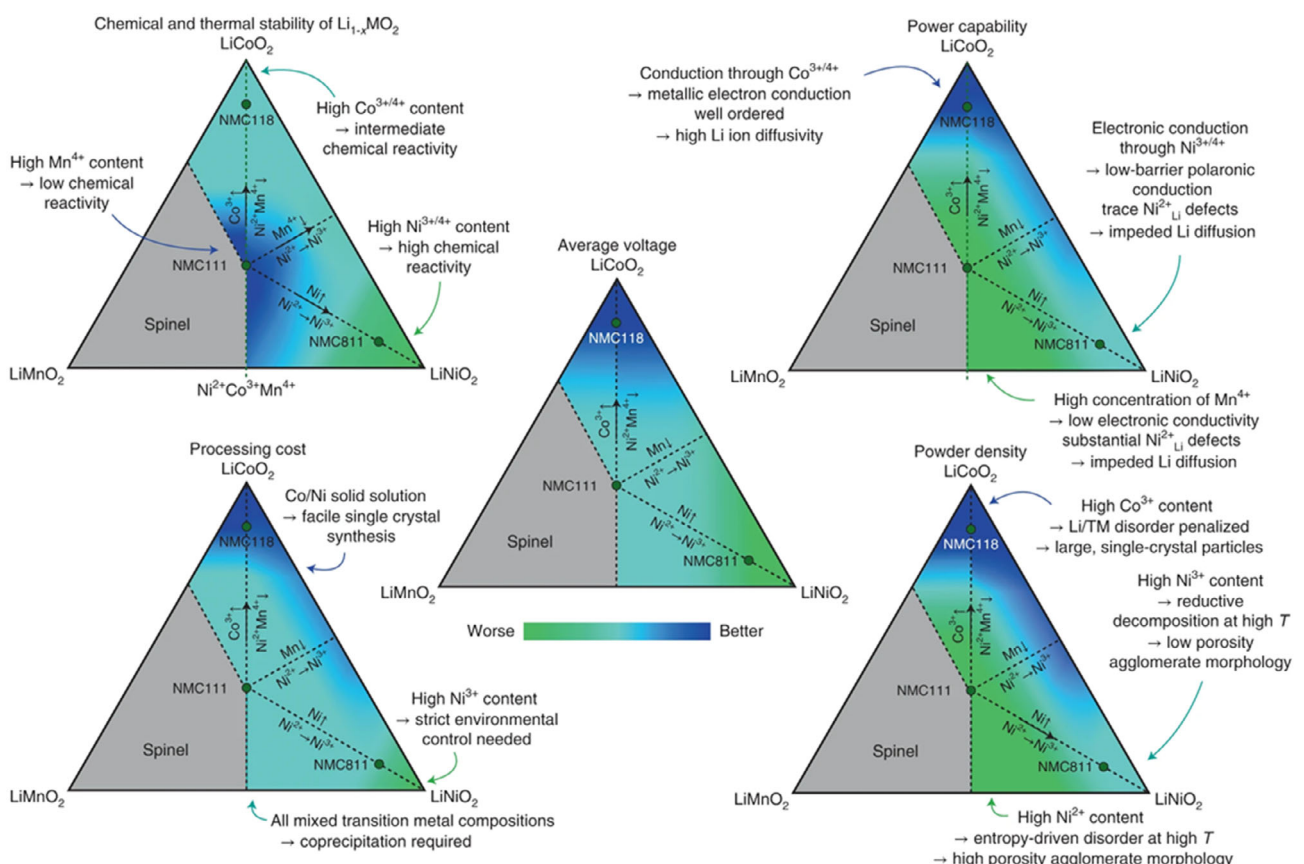


Figure 6. Phase diagrams of LiCoO₂, LiNiO₂ and LiMnO₂ based on (chemical and thermal) stability, power capability, average voltage, processing cost, and powder density. Reproduced with permission.^[38] Copyright 2022, Springer Nature.

hexagonal LiMO_2 (R-3m) at the nanoscale and 2) a single monoclinic phase $\text{Li}(\text{Li}_{1/3-2x/3}\text{M}_x\text{Mn}_{2/3-x/3})\text{O}_2$ and an excess of lithium ions in the TM layer. There has been much controversy over the structure of lithium-rich layered materials. However, regardless of which form it belongs to, it has an O3-type structure.

Figure 7a shows the charge and discharge curve of the lithium-rich layered material in the first circle.^[40] The first circle curve can be divided into three regions, where region 1 corresponds to the oxidation of TM ions in the LiMO_2 component, region 2 is the delithium of the Li layer in Li_2MnO_3 , and region 3 is the delithium of the TM layer in Li_2MnO_3 . However, the source of the lithium-rich manganese base capacity has been a big dispute. Some researchers believe that the high capacity originates from the electrochemical reaction of $\text{Mn}^{4+/5+}$; however, this charging voltage is lower than the equilibrium potential of Mn^{4+} to Mn^{5+} (5.1 V vs. Li^+/Li), so there is an implausibility of the $\text{Mn}^{4+/5+}$ mechanism. Recently, Radin et al.^[41] proposed a charge compensation mechanism for Mn^{7+} using first-principles calculations driven by phase diagrams. However, this mechanism lacks intuitive experimental data and requires further in-depth study. The energy band diagram in Figure 7b,c shows that in stoichiometric oxides (such as high-nickel layered oxides), the d electrons of a TM are hybridized with the p electrons of ligand oxygen. And there is a correlation between the redox reaction and the position of the Fermi energy level.^[42] Thus, while charging high-Ni layered oxides, electrons below the Fermi energy level (i.e., d-electrons in

e.g., or t_{2g}) are only extracted by a single TM redox. However, for lithium-rich layered oxides, p electron coordination is insufficient due to the lack of d electrons in the cellular superlattice of Li. As a result, the oxygen p-electrons pointing to Li exist as O_{2p} non-bonding orbitals in the energy band diagram, leading to anionic redox.^[42] Seo et al.^[43] systematically studied the local atomic coordination around oxygen in stoichiometric lithium and lithium-rich. The results show that the main difference between them is the Li-O-X configuration. As shown in Figure 7d,e, the Li-O-Li configuration in lithium-rich oxides leads to the redox activity of the unhybridized O^{2p} state, which provides capacity through the oxidation reaction of O^{2-} . Although the source mechanism of Li-rich capacity has been extensively studied, its internal mechanism has not been unified. In addition, lithium-rich cathode faces the problems of rapid capacity/voltage decay, serious oxygen precipitation and irreversible structural transformation, which seriously hinders its commercialization process.

2.2. Spinel Structure Cathode Material

Spinel structure LiM_2O_4 cathode material belongs to the cubic crystal system, Fd-3m space group. Taking LiMn_2O_4 as an example, Li^+ and $\text{Mn}^{3+/4+}$ occupy the 8a tetrahedral position and 16d octahedral position of the spinel structure, respectively, and oxygen ions are face-centered cubic densely packed.^[44] In the structure, a stable $[\text{Mn}_2]_{16d}\text{O}_4$ frame with a shared octahedron

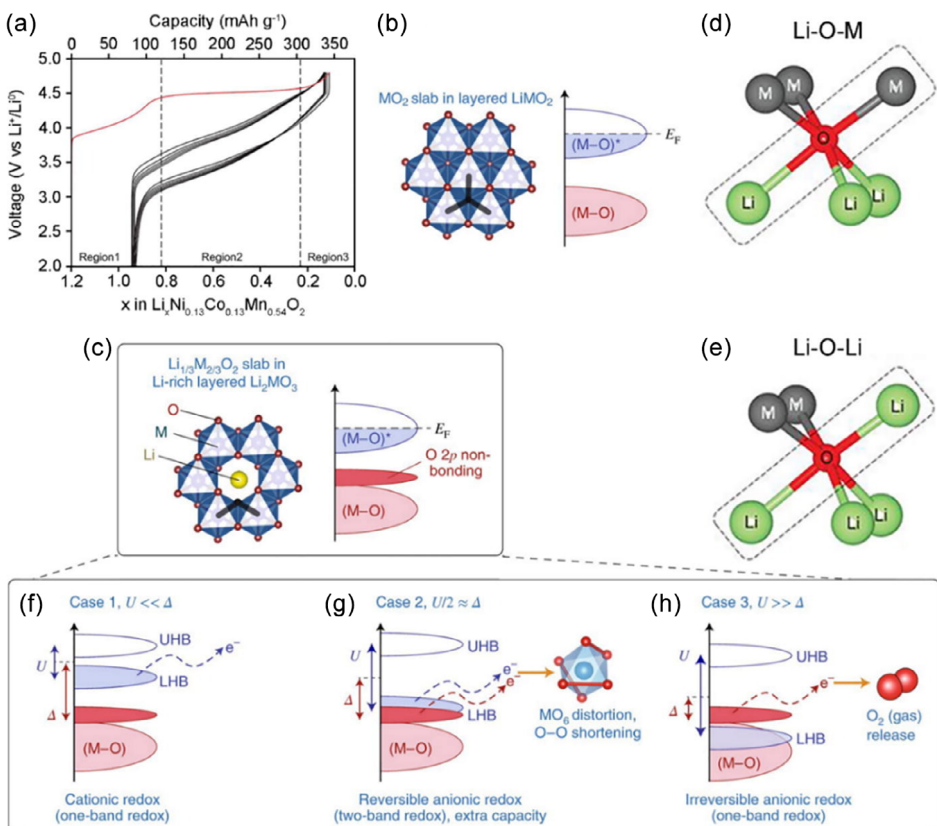


Figure 7. a) Charge/discharge curves of $0.5\text{Li}_2\text{MnO}_3\cdot0.5\text{LiTMO}_2$ at 0.2 C. b,c) Energy band structure of layered oxides; local atomic coordination around oxygen in d) stoichiometric lithium and e) lithium-rich. f-h) Energy band structure of lithium-rich oxides in the three cases. Reproduced with permission.^[43] Copyright 2021, Elsevier.

can provide a 3D path for the rapid diffusion of Li^+ . Moreover, Mn-Mn can promote electron conduction through the direct interaction of sharing the MnO_6 octahedral edge and the high-spin $\text{Mn}^{3+/4+}$: $t_{2g}^3 e_g^{1-x}$ in $(\text{Li}_{1-x})_{8a}[\text{Mn}_2]_{16d}\text{O}_4$. Thus, LiMn_2O_4 has a specific capacity of 130 mAh g^{-1} at an operating voltage of about 4.0 V. In addition, LiMn_2O_4 also has the advantages of low cost, green environmental protection, and good thermal stability. However, in the actual discharge process, part of the lithium ions at the 8a tetrahedral site will spontaneously embed into the 16c octahedral vacancy, decreasing operating voltage.^[24] In addition, a single e.g., electron in the high-spin state Mn^{3+} : $t_{2g}^3 e_g^1$ will cause the Jahn-Teller effect, which causes the irreversible transformation of the crystal structure from the cubic phase to the tetragonal phase, and the two reverse effects will cause drastic changes in the c/a ratio and the cell volume, which aggravate the performance attenuation.^[45] Another critical issue of LiMn_2O_4 is that in the presence of trace (ppm level) hydrogen ions (acidic) in the electrolyte, the disproportionation reaction of Mn^{3+} produces Mn^{2+} and Mn^{4+} , which results in severe Mn leaching.^[36,46] Mn leaching not only exacerbates the structural degradation of the cathode but also damages the graphite anode, which in turn shortens the cycling life of Li-ion batteries.^[37] In order to improve the cyclic stability of LiMn_2O_4 , the researchers used Cr, Co, and Ni to dope it, among which Ni-doped $\text{LiNi}_{0.5}\text{Mn}_{1.5}\text{O}_4$ is considered the most promising high-pressure spinel material. In this structure, Mn is +4-valent, and Ni is +2-valent.^[47] As a result, $\text{LiNi}_{0.5}\text{Mn}_{1.5}\text{O}_4$ has $\text{Ni}^{2+/3+}$ and $\text{Ni}^{3+/4+}$ redox pairs as well as tetrahedral lithium ions, which can release a reversible specific capacity of 135 mAh g^{-1} at an operating voltage of $\approx 4.7 \text{ V}$.^[24] However, due to the lack of a suitable high-voltage electrolyte, the $\text{LiNi}_{0.5}\text{Mn}_{1.5}\text{O}_4$ cathode has a serious capacity attenuation.

2.3. Disordered Rock Salt Oxide Cathode Material

Usually, the structure of the cation disorder is thought to hinder the migration of lithium ions, making it unsuitable as a cathode material. Recent studies have shown that lithium-rich cationic disordered materials have high capacity and good stability.^[48,49] The crystal structure of the disordered rock salt positive electrode can be described as a "layered structure with randomly disordered cations," that is, Li ions and TM ions are randomly distributed in the crystal structure, and the distinction between the two layers is not obvious (Figure 8a). As shown in Figure 8b,c, in the material with a cationic disorder of $\text{Li}_{1.211}\text{Mo}_{0.467}\text{Cr}_{0.3}\text{O}_2$, the diffraction peak intensity of (003) decreases significantly at the 10th cycle, indicating that the material has a large cationic disorder. Although the degree of disorder of the crystal structure of the material has increased, a large number of Li ions can still be reversibly removed/inserted. This reversible Li-ion removal/embedding results from permeable 0-TM networks.^[50] When the intermediate tetrahedral site is not coplanar with the octahedral transition metal ion, a 0-TM permeable network can be formed. To achieve fast macroscopic diffusion, 0-TM channels must be continuously connected throughout the material to form a permeable network. As shown in Figure 9d, Lee et al.^[51] calculated by density functional theory and found that the increase of

Li metrological ratio can provide more 0-TM channels for the 0-TM penetration network and enhance the continuity of the network. Similar to lithium-rich layered cathode, although the redox reaction of O ions will bring higher specific capacity, it will also cause irreversible loss of first ring capacity and rapid performance degradation. Moreover, surface oxygen loss densifies the lattice, thus blocking the 0-TM permeation network and intensifying electrochemical polarization. In addition, the formation of O-O bonds and O-vacancies cause the dissolution of transition metal ions and loss of capacity. At present, researchers have developed a variety of (such as Mn-based, Ti-based, Nb-based, and Mo-based) lithium-rich disordered rock salt oxide cathode but still cannot reasonably explain its structural evolution, charge compensation mechanism, and ion transport characteristics, so it is still in the basic research stage.

3. Research Progress of High-Nickel Ternary Layered Cathode Materials

Compared with LiCoO_2 (LCO) cathode material, LiNiO_2 (LNO) cathode has the advantages of high specific capacity, abundant resources, and lower cost. However, LNO has some key problems, such as serious $\text{Li}^+/\text{Ni}^{2+}$ mixing, difficult synthesis, irreversible H2-H3 phase transition, and poor safety, which hinder its commercial application. By introducing transition metal ions such as Co, Mn, Al, Ti, Mg, and Mo into LNO to form binary or ternary layered oxides of different proportions, the researchers improved the material's structural stability and cycle stability. The NCM ternary positive electrode with higher energy density is constructed by flexibly adjusting the composition of Co and Mn. In 1999, Liu et al.^[52] first reported a series of $\text{LiNi}_{0.7}\text{Co}_{0.2}\text{Mn}_{0.1}\text{O}_2$, $\text{LiNi}_{0.6}\text{Co}_{0.2}\text{Mn}_{0.2}\text{O}_2$, and $\text{LiNi}_{0.5}\text{Co}_{0.2}\text{Mn}_{0.3}\text{O}_2$ cathode materials. It is also proposed that the doping of Co and Mn can improve the nonstoichiometric ratio characteristics and optimize the cycle stability of LNO materials (Figure 1–10). Subsequently, in 2000, Yoshio et al.^[53] prepared $\text{LiNi}_{1-x-y}\text{Co}_y\text{Mn}_z\text{O}_2$ ($x \leq 0.2$, $0 \leq y \leq 0.3$) cathode material with a capacity of more than 155 mAh g^{-1} . However, in earlier studies, researchers did not realize the importance of regulating the composition of NCM materials. Until 2001, Ohzuku and Makimura et al.^[54] prepared $\text{LiNi}_{1/3}\text{Co}_{1/3}\text{Mn}_{1/3}\text{O}_2$ cathode material (NCM111) with the same transition metal content. The study found that compared with LCO, NCM111 can not only provide a reversible capacity of 160 mAh g^{-1} but also has higher safety performance. After the initial implementation of NCM111, researchers gradually realized the importance of NCM material components and then reported the $\text{LiNi}_x\text{Co}_{1-2x}\text{Mn}_x\text{O}_2$ series of cathode materials.

The low-nickel NCM material exhibits better thermal stability and higher energy density, but the capacity is limited to 200 mAh g^{-1} . Therefore, increasing Ni content and decreasing Mn/Co content is an effective way to increase capacity. In 2005, Liao et al.^[55] reported a series of $\text{LiNi}_{0.75-x}\text{Co}_{0.25}\text{Mn}_x\text{O}_2$ ($0.1 \leq x \leq 0.25$) cathode materials, among which $\text{LiNi}_{0.6}\text{Co}_{0.25}\text{Mn}_{0.15}\text{O}_2$ showed the best electrochemical performance, and the specific first-circle discharge capacity was 167 mAh g^{-1} . Subsequently, Kim et al.^[56]

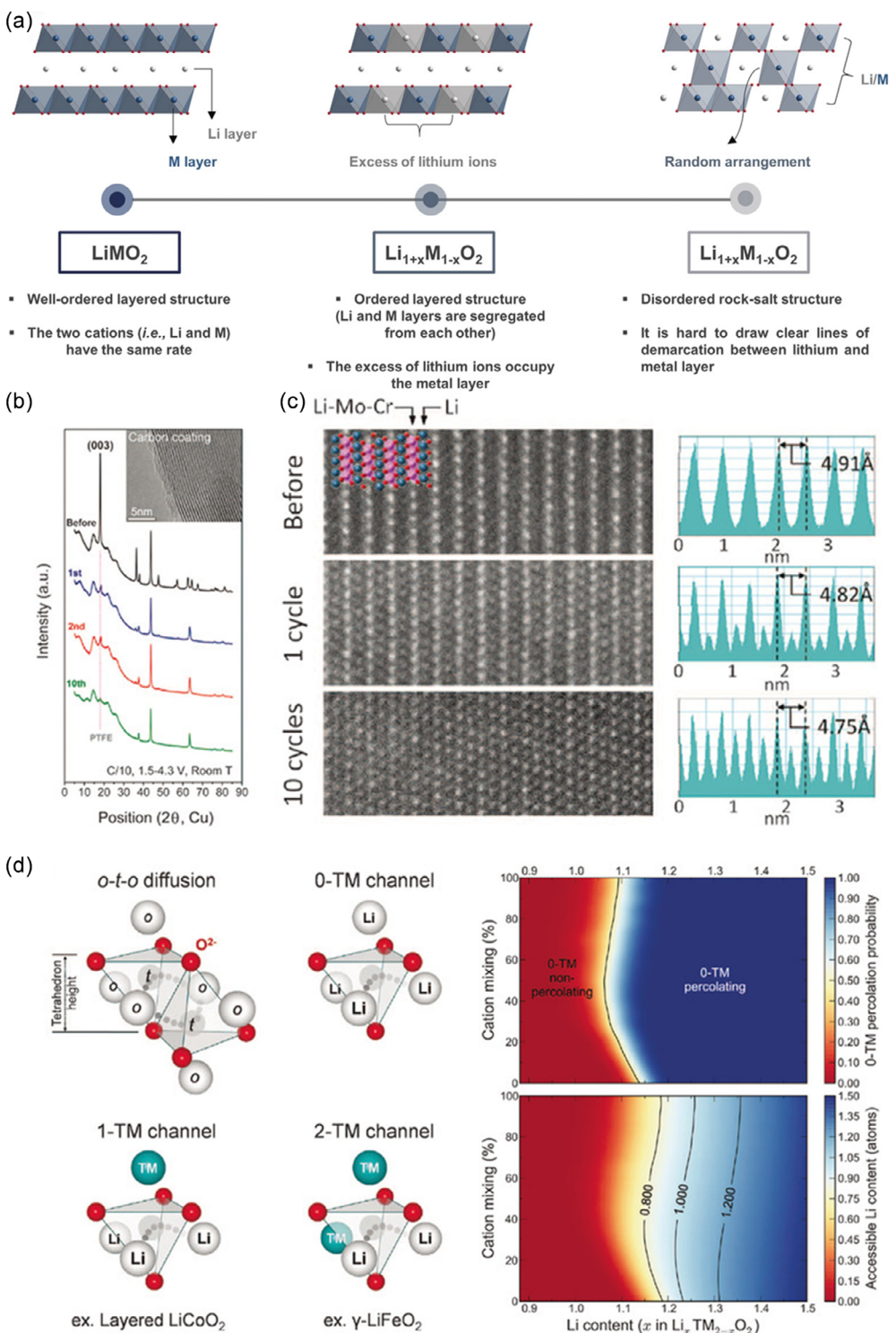


Figure 8. a) Schematic illustrations of ordered and disordered layered structures; b) X-ray diffraction (XRD) patterns and c) STEM images of Li_{1.211}Mo_{0.467}Cr_{0.3}O₂ cathodes at different cycle numbers; d) Possible paths for o-t-o diffusion and the probability of finding a percolating network of 0-TM channels in rock salt phase oxides in relation to Li content and cation mixing. Reproduced with permission.^[51] Copyright 2020, Wiley-VCH.

prepared spherical LiNi_{0.8}Co_{0.1}Mn_{0.1}O₂ and LiNi_{0.8}Co_{0.2}O₂ cathode materials by coprecipitation combined with solid phase sintering, which had a discharge-specific capacity of about 200 mAh g⁻¹. It is found that adding a small amount of Mn to the system can improve the material's structural and thermal stability. Since then, the Co and Mn ratio regulation in the NCM system has

gradually received attention. In 2009, Li et al.^[57] systematically compared the electrochemical properties and thermal stability of LiNi_{0.6}Co_xMn_{0.4-x}O₂ ($x = 0.05, 0.10, 0.15$ and 0.2). The results show that the capacity of the material increases monotonously with the increase of the proportion of Co in the system. Still, with the decrease in Mn content, the material's cyclic performance and

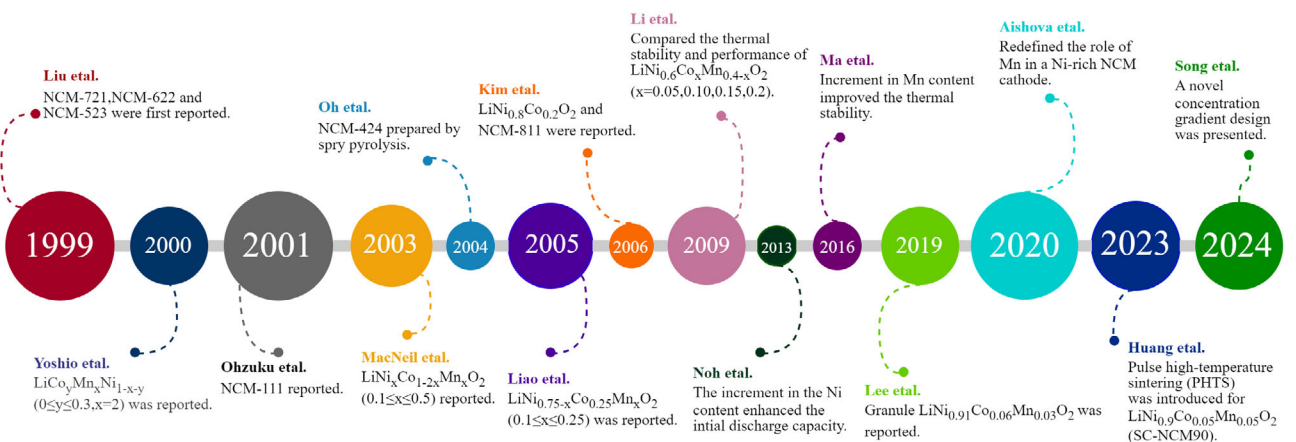


Figure 9. The development history of nickel-rich cathode materials. Adapted from ref. [69] Copyright 2022, Wiley-VCH.

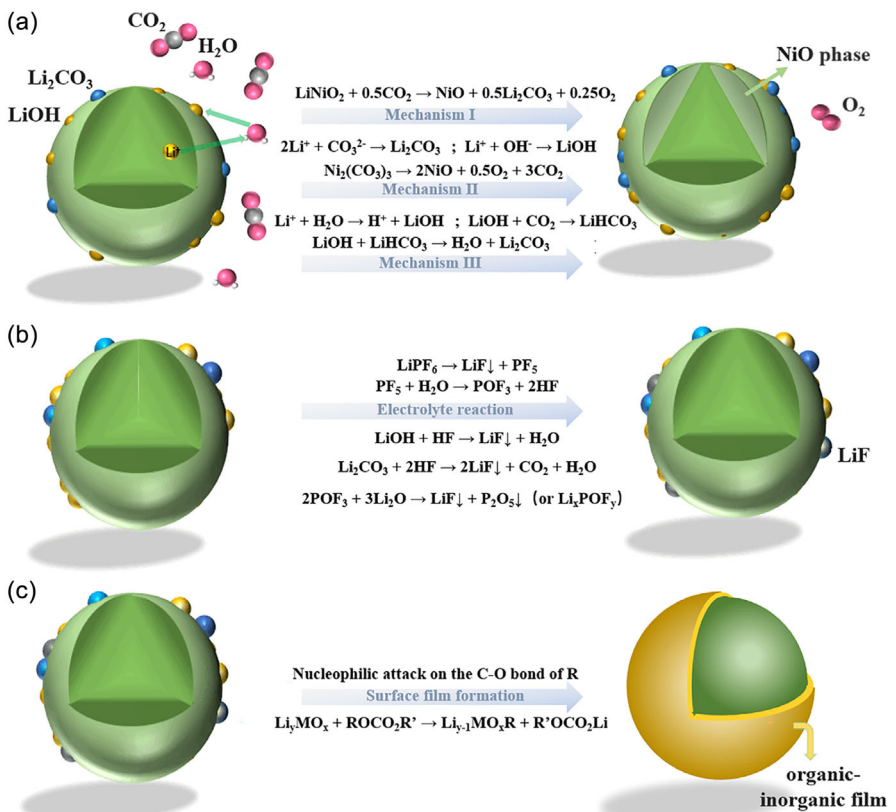


Figure 10. a) Scheme of the formation of surface residual lithium for nickel-rich cathode material; b,c) Scheme of the surface structure degradation during the cycling process. Reproduced with permission.^[23] Copyright 2023, Elsevier.

thermal stability gradually deteriorate. In 2013, Noh et al.^[58] found that the initial discharge capacity of materials increased with the increase of Ni content by comparing NCM with different Ni content. Liu et al.^[59] systematically summarized the synergy between $\text{LiNiO}_2\text{-LiCoO}_2\text{-LiMnO}_2$ in NCM cathode materials, and the results showed that the material capacity was basically derived from $\text{Ni}^{2+/3+/4+}$ redox electric pairs. Mn ion always maintains +4 valence so that it can improve structural stability and thermal stability. The t_{2g} orbitals of Co^{3+} overlap with O 2p orbital in part, resulting in stronger electron delocalization, thus helping to

improve the conductivity and magnification properties of the material.^[59]

In recent years, with the increasing requirements on the endurance history of electric vehicles, the development of power batteries with higher energy density has become the first choice, so ultrahigh-nickel NCM ($\text{Ni} \geq 0.9$) with higher nickel content has gradually become a hot research field.^[60] In 2019, Aishova et al.^[61] systematically studied the physicochemical properties of $\text{LiNi}_{0.9}\text{Co}_{0.05}\text{Mn}_{0.05}\text{O}_2$ (NCM90), $\text{LiNi}_{0.9}\text{Mn}_{0.1}\text{O}_2$ (NM90), and $\text{LiNi}_{0.9}\text{Co}_{0.1}\text{O}_2$ (NC90). The results show that NM90 has the best

cyclic stability. When the temperature reached 60 °C, NM90 showed a similar magnification performance to NCM90. Recently, in order to obtain a better comprehensive performance of the cathode material, Kim et al.^[62] synthesized LiNi_{0.89}Co_{0.05}Mn_{0.05}Al_{0.01}O₂ quaternary cathode material (NCMA) based on the ternary cathode, which has the first discharge specific capacity of 228 mAh g⁻¹ and shows good cycle stability. Huang et al.^[63] proposed a novel synthesis method for single-crystal LiNi_{0.9}Co_{0.05}Mn_{0.05}O₂(SC-NCM90) in 2023, termed pulse high-temperature sintering (PHTS). Compared to NCM90 sary spheres, SC-NCM90 demonstrated a 1/3 increase in tap density, reaching 2.76 g cm⁻³, and it showed an initial capacity of 209 mAh g⁻¹. The formation of microcracks was effectively suppressed during cycling. In 2024, Song et al.^[64] introduced a nickel-rich ternary cathode material with a concentration gradient structure (CG-NCM), which significantly enhanced its cycling stability and thermal stability through a core–shell design. The material features a nickel-rich core for high energy density and a high-manganese shell for structural robustness. CG-NCM demonstrated outstanding performance under high-rate and high-voltage conditions, with a markedly extended cycle life and reduced side reactions between the electrolyte and the nickel-rich core. In general, high-nickel ternary cathode has gradually become a hot spot in academic research and industrial production. However, how to balance the energy density, safety, and production cost of cathode materials needs further in-depth research.

3.1. Problems Existing in High-Nickel Layered Cathode Materials

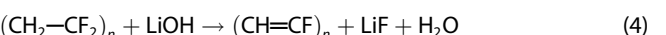
Although high-nickel ternary cathode materials have great development prospects, they face problems such as sharp performance attenuation and large safety risks, so their practical application is still severely limited. At present, the main problems faced by high-nickel ternary cathodes can be classified as follows: 1) the formation of residual lithium during material preparation and storage; 2) cationic mixing caused by material synthesis and battery cycle; 3) the irreversibly layer-spinel-salt phase transition and lattice oxygen vacancy induced structural reconstruction; 4) release of O₂ and CO₂ caused by structural rearrangement and side reactions at the interface; 5) dissolution of transition metal ions; 6) formation of intrachrystalline and intergranular microcracks; 7) poor thermal stability.

3.1.1. Surface Residual Lithium

Residual lithium compounds such as Li₂O, Li₂O₂, LiHCO₃, LiOH, and Li₂CO₃ inevitably form on the material's surface during the high-nickel cathode materials' preparation process. They are eventually transformed into LiOH and Li₂CO₃ during storage (Figure 10a).^[65] The residual lithium impurities mainly originate from residual lithium and released lithium. On the one hand, during the synthesis process, additional Li sources need to be added to compensate for the loss of Li due to high temperatures and to reduce the cationic mixing of the material, thus resulting in a small amount of residual lithium that fails to react completely will

exist in the form of Li₂O and react directly with CO₂ and H₂O in the air during the storage process, leading to the formation of Li₂CO₃ and LiOH.^[34] On the other hand, the surface of the high-nickel cathode material is highly alkaline and extremely sensitive to H₂O and CO₂ in the air, so when the material is in contact with the air, the particle surface will slowly react to form residual lithium substances. The reaction mechanism can be divided into the redox reaction mechanism and the Li⁺-H⁺ exchange mechanism. In the redox mechanism, Ni³⁺ on the particle surface is spontaneously reduced to Ni²⁺, producing oxygen ions with high reactivity(O₂-active).^[66] Highly reactive oxygen ions will react with H₂O and CO₂ in the air to form OH⁻ and CO₃²⁻ and then react with Li⁺ to form residual lithium compounds. The exchange mechanism of Li⁺-H⁺ is that Li⁺ precipitated from the lattice will adsorb water molecules in the air and exchange with H⁺, resulting in the formation of LiOH, and the subsequent reaction with CO₂ leads to the formation of Li₂CO₃.^[67,68]

The presence of residual lithium material on the surface of high-nickel materials causes two main problems: 1) the gelation of the paste during the cathode coating and 2) severe gas production leads to battery expansion. The first problem is that due to the defluorination reaction of PVDF in the alkaline environment of LiOH and the formation of H₂O and the C=C unsaturated bond of cross-linked polymerization (as shown in Formula 1–4), the generated H₂O will make PVDF gel and jelly quickly, resulting in the difficulty of uniform coating of the slurry on the collector.^[69] The second problem is that Li₂CO₃ will be electrochemically oxidized at a high potential, generating CO₂ and O₂, as described in Equation (5).^[69] In addition, residual lithium compounds also react directly with organic solvents and LiPF₆ in the electrolyte, forming H₂O and CO₂. The trace amount of H₂O, a side reaction product, will further induce the decomposition of LiPF₆ and form HF and other by-products.^[70,71] The reaction generated by HF will further aggravate the decomposition of surface residual lithium, such as Li₂CO₃ and LiOH. HF will erode the material's surface, resulting in the dissolution of transition metal ions and eventually leading to the rapid deterioration of the surface structure and the sharp decay of the capacity (Figure 10b,c).



During the preparation of the cathode material, the residual lithium substance formed can hardly be completely removed. Acid or aqueous solution cleaning reduces the residual lithium content on the particle surface.^[72,73] In addition, the removal of surface residual lithium can also be achieved by coating; the mechanism of action is to reduce the residual lithium by reacting with an acidic coating agent. And high-temperature heat treatment can also be used to reduce the residual lithium content.

3.1.2. Cationic Mixing

Similar to LiNiO₂, there are relatively serious Li⁺/Ni²⁺ mixed arrays in high-nickel ternary cathode materials.^[74] This cationic mixing not only occurs in the preparation process but also accumulates

gradually during the cycle, causing the material to gradually change from the ordered layered structure to the disordered spinel phase and rock salt phase, resulting in a sharp decline in electrochemical performance. In addition, $\text{Li}^+/\text{Ni}^{2+}$ mixing can also lead to a decrease in the diffusion coefficient of the system Li^+ because the migration of lithium ions with a larger ionic radius to the transition metal layer will increase the transition metal layer spacing and reduce the lithium layer spacing. The transition metal ions occupying the lithium site hinder the diffusion of lithium ions through electrostatic repulsion. Generally, the degree of cation mixing can be preliminarily judged by the $I_{(003)}/I_{(104)}$ ratio of X-ray diffraction.^[69,75] However, because the diffraction peak intensity of XRD is proportional to the atomic number, it is difficult to analyze lithium atoms with lighter mass and smaller radius quantitatively. Neutron powder diffraction (NPD) is more sensitive to the detection of lithium atoms so that it can be used for quantitative analysis of the degree of cation mixing. Xiao et al. systematically studied a series of layered cathode materials using NPD.^[76] The results show that the degree of $\text{Li}^+/\text{Ni}^{2+}$ mixing is gradually intensified with the increase of Ni proportion in the system.

Although a large number of studies have shown that $\text{Li}^+/\text{Ni}^{2+}$ mixing can reduce structural stability and exacerbate performance degradation, the origin of $\text{Li}^+/\text{Ni}^{2+}$ mixing is still unclear. Some studies attributed the Ni/Li exchange in layered TM oxides to the similar size of Ni^{2+} and Li^+ . When the sizes of the alkali metal (A) and transition metal (M) cations were similar, they would be distributed on the sites of a perfect rocksalt lattice, and the $\alpha\text{-LiFeO}_2$ structure was more stable due to its lower electrostatic energy. In contrast, as the size difference between the cations increases, the $\alpha\text{-NaFeO}_2$ structure became more stable because it allowed for more optimal relaxation of the cation-oxygen bond lengths.^[77] However, the spatial effect is difficult to explain, and high-nickel ternary materials with more Ni^{3+} content show more severe $\text{Li}^+/\text{Ni}^{2+}$ mixing. Recently, Zheng et al.^[78] conducted a detailed study on the origin of $\text{Li}^+/\text{Ni}^{2+}$ mixing: 1) based on the relaxation mechanism of $\alpha\text{-NaFeO}_2$ and $\alpha\text{-LiFeO}_2$ structures, spatial interaction is one of the driving forces of $\text{Li}^+/\text{Ni}^{2+}$ mixing; 2) the linear superexchange configuration of interlayer $\text{Ni}^{2+}\text{-O}^{2-}\text{-Ni}^{2+}/\text{Mn}^{4+}$ also provides driving force for $\text{Li}^+/\text{Ni}^{2+}$ mixing; 3) the lower migration energy barrier of Ni^{2+} provides kinetic energy advantage for $\text{Li}^+/\text{Ni}^{2+}$ mixed platoon. In addition, Wang et al.^[79] found that cobalt (Co) substitution promotes the ordering of lithium (Li) and nickel (Ni), alleviates magnetic frustration, and reduces superexchange interactions, thereby decreasing Li/Ni mixing. In contrast, manganese (Mn) substitution exacerbates Li/Ni mixing by enhancing magnetic frustration and superexchange interactions. Experimental results showed that as the Mn content increased, the lattice parameters a and c enlarged, and the degree of Li/Ni mixing intensified. Theoretical calculations further revealed the crucial role of magnetic interactions in regulating Li/Ni mixing, indicating that the effects of magnetic frustration and superexchange interactions on Li/Ni mixing are much greater than those of changes in ionic radii. All these theories can better explain why high-nickel ternary materials dominated by Ni^{3+} have a more serious $\text{Li}^+/\text{Ni}^{2+}$ mixed arrangement.

3.1.3. Oxygen Evolution Reaction (OER) and Gas Production

At high potential, lattice oxygen will participate in redox reaction for charge compensation, which leads to oxygen precipitation in the material and further induces structural transformation. At present, the underlying mechanism of OER remains unclear. Flores et al.^[80] used *in situ* Raman and density functional theory (DFT) to analyze the correlation between lattice oxygen and M—O bond in $\text{Li}_x\text{Ni}_{0.8}\text{Co}_{0.15}\text{Al}_{0.05}\text{O}_2$ at different lithium states. The results show that when $x \approx 0.2$ is charged to about 4.2 V (corresponding to $\text{H}_2 \rightarrow \text{H}_3$ phase transition), the covalency of the M—O bond in the highly hybrid state of electrons will be enhanced, and lattice oxygen is more likely to participate in the reaction to provide charge compensation, so as to be oxidized out. Based on the 633 nm photon emission strategy generated by ${}^1\text{O}_2$ deactivation, Wandt et al.^[81] detected highly active singlet oxygen intermediates in highly detoxified NCM materials, providing a theoretical basis for oxygen precipitation in high-nickel cathode materials. However, Zhang et al.^[82] attributed OER at high potential to the thermodynamic instability of the H_3 phase itself, which belongs to the intrinsic phenomenon of materials. The high voltage capacity is due to the oxidation of Ni and O anions. Due to the limitation of oxygen diffusion kinetics, OER mainly occurs on the surface of the material rather than inside the material.

The OER will not only intensify the gas production of the battery, but also the reactive oxygen generated by the reaction will further react with the electrolyte solvent and generate CO and CO_2 , which will not only increase the battery impedance but also cause the structure of the material to irreversibly change from the ordered layered structure to the disordered spinel/rock salt phase. In addition, the generated CO_2 will undergo a reduction reaction on the anode, resulting in the consumption of active lithium ions in the system and the reduction of the anode/cathode capacity ratio, which will eventually lead to positive overcharge and aggravate structural degradation.^[82] Therefore, OER is a major source of cathode structure degradation, electrolyte solvent consumption, and battery safety problems. In addition to the above OER, the following reasons can also cause the battery gas production: 1) the side reaction between the electrode and the electrolyte, 2) Li_2CO_3 decomposition and reaction with electrolyte products, and 3) oxidation of electrolyte.^[83] Serious gas production will increase the internal pressure of the battery, resulting in mechanical deformation of the battery structure and affecting its safety.

3.1.4. Phase Transformation

When the high-nickel cathode material is in a deeply detoxified state, its structure is relatively unstable, and some transition metal ions migrate through the oxygen tetrahedral site and occupy the lithium site, thus resulting in a laminar-spinel-halite phase transition in the structure, accompanied by oxygen precipitation.^[84] In addition, the phase transition is anisotropic and occurs through the following steps: first, the oxidation of $\text{Ni}^{2+}/\text{Ni}^{3+}$ and Co^{3+} and the decomposition of the electrolyte produce by-products such as O^- , O_2^- , O_2^{2-} , and O_2 on the cathode surface.^[69] However, the

formation of oxygen defects in the crystal structure will reduce the energy barrier of transition metal(Ni/Mn/Co) to the lithium site, resulting in the gradual accumulation of cationic mixing during the cycle, and eventually, the structure changes from lamellar(R3-m) to spinel phase (Fd-3m).^[85,86] With the gradual deterioration of the structure, Co, with similar properties to Ni, also has the ability to migrate in the high oxidation state, so it will gradually migrate from the transition metal octahedral position through the oxygen tetrahedral position to the lithium octahedral position, resulting in the formation of the rock salt(Fm-3m) phase with poor lithium ion dynamics, and eventually lead to the increase of internal resistance and sharp capacity attenuation of the battery.^[87] A large number of research results show that with the increase in Ni content, temperature, and SOC, structural stability decreases significantly.^[69]

3.1.5. Transition Metal Ion Dissolution

The dissolution of transition metal ions is similar to phase transition and is the result of the combined action of OER and cationic mixed expulsion.^[69,88,89] OER and mixed cation can result in loss of lattice oxygen and formation of lower-priced transition metal cations. Compared with high-valence cations, low-valence cationic salts have greater solubility in liquid electrolytes, thus causing serious transition metal ion leaching. The precipitation of oxygen will catalyze the decomposition of electrolyte solvent, resulting in the formation of CO, CO₂, and H₂O. At the same time, H₂O will intensify the decomposition of LiPF₆ electrolyte solution and form HF, thus further aggravating the dissolution of transition metal ions.^[90]

The influence of transition metal ion dissolution on battery performance is mainly reflected in the following two aspects: 1) the loss of active transition metal ions, resulting in the decrease of operating voltage and capacity attenuation, and 2) transition metal ions migrating to the anode will not only intensify solvent reduction but also form an inert inorganic layer on the anode surface.^[91] The decrease in solvent will cause a decrease in cathode/anode capacity, and the increase in SEI film thickness will cause an increase in impedance, which will cause the attenuation of battery performance. In addition, dissolved transition metal ions are transported to the graphite anode surface and reduced to elemental metals during subsequent electrochemical reactions.^[92] The resulting metals can puncture the diaphragm, short-circuit the battery, and cause thermal runaway.

3.1.6. Microcrack

In high-nickel ternary cathode materials, an important factor leading to capacity attenuation is the formation and expansion of microcracks in the particles. During the cyclic process, the H₂-H₃ phase transition leads to severe and anisotropic lattice contraction/expansion, which leads to the accumulation of local intergranular/intragranular stress and strain, resulting in the formation and expansion of intergranular and intragranular microcracks, and ultimately the deterioration of cathode structure and properties.^[93] As shown in Figure 11a,b, higher cut-off voltage and nickel content in NCM will aggravate the formation of microcracks.^[94,95] Taking LNO

as an example, as shown in Figure 11c,d, LNO underwent a series of structural evolution and lattice parameter changes during the process of delithium.^[30] With the decrease of lithium content in Li_xNiO₂, Ni³⁺ is gradually oxidized to Ni⁴⁺, the lattice parameter *a* decreases monotonically, and the value of *c* increases and then sharply decreases.^[96,97] This phenomenon is because when Li⁺ is removed from the structure, the electrostatic repulsion force between NiO₂ layers will increase, so the interlayer distance increases and the *c* value increases. When *x* increases to 0.36, the lattice constant *c* decreases sharply due to two factors: 1) the enhancement of the covalent bond in the Ni₄₊-O₂ layer reduces electrostatic repulsion, and 2) with the decrease of Li content in the Li layer, the pillar effect gradually weakens.^[98,99] Such a repeated phase transformation process will lead to the continuous formation of microcracks, which will gradually extend from the inside of the particle to the outside along the grain boundary. The effects of microcracks on materials mainly include two aspects: 1) the formation of microcracks leads to the loss of direct electrical contact between adjacent primary particles, resulting in increased resistance and attenuation of the final battery performance, and 2) the formed microcracks provide more active sites for the internal particle side reactions, thus intensifying the interfacial side reactions and generating an electrochemically inert NiO-like phase, hindering lithium ion diffusion and increasing resistance. At the same time, the formation of microcracks will also aggravate the uneven distribution of SOC inside the material, trigger the heterogeneity of the system reaction, further induce the formation of microcracks, and finally lead to the fragmentation of particles and the sharp attenuation of performance.^[100,101]

3.1.7. Safety Problem

Safety is one of the main reasons that hinder the further commercialization of high-nickel cathode materials. In the process of charge and discharge, when the heat dissipation rate of the battery is far from meeting the heat production rate, a large amount of heat will gradually accumulate inside the battery structure and finally cause the battery thermal runaway.^[102] Thermal runaway can trigger a chain reaction such as smoke, fire, and explosion. The occurrence of these reactions will also exacerbate thermal runaway, which seriously threatens the safety of the battery. The main causes of thermal runaway are mechanical, electrochemical, and thermal abuse.^[93] Mechanical impingement or growth of lithium dendrites can cause a short circuit inside the battery, resulting in a dramatic release of heat. In addition, high external ambient temperature or unscientific heat dissipation structure design will also cause the accumulation of internal heat in the battery, leading to thermal runaway.^[93] At the material scale, the poor thermal stability of the high-nickel positive electrode is due to the low M-O bond strength in the delithium state, and the binding energy decreases with the increase of Ni content or the amount of removed lithium.^[103] Therefore, in a highly delithiated state, oxygen evolution and Ni reduction reactions are more likely to occur, resulting in the release of heat. Recently, Yoon et al.^[104] used X-ray absorption near-side structure

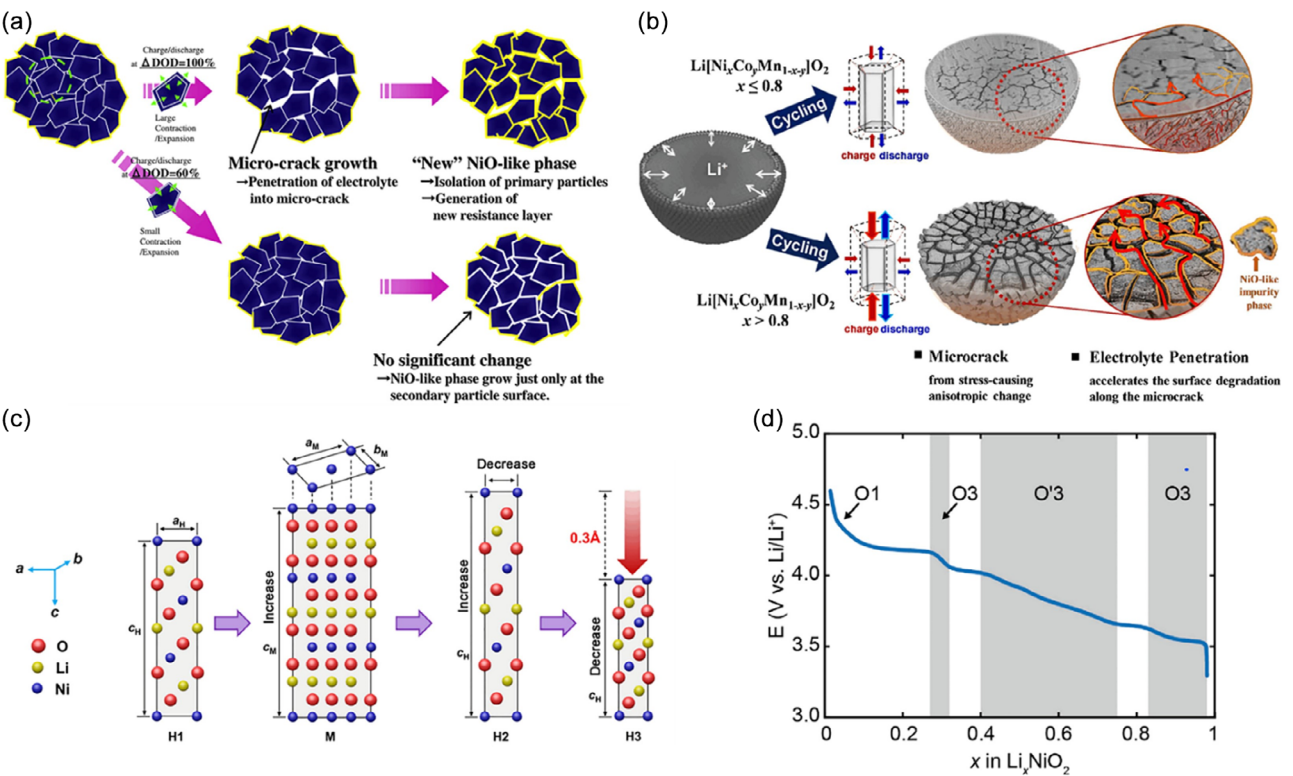


Figure 11. a) The relationship between deeply discharge state and microcrack generation. b) The effect of different content of nickel on microcrack generation at the same discharge state. c) The phase change of LiNiO_2 during the initial charge. d) The voltage profile of Li_xNiO_2 and the corresponding phase. Reproduced with permission.^[23] Copyright 2023, Elsevier.

(XANES) characterization to reveal that thermal expansion and oxygen vacancy have a great impact on the thermal stability of materials. The results show that Ni^{4+} has a serious reduction reaction at higher temperatures, accompanied by a large number of oxygen vacancies. Due to the change of lattice constant, the charged cathode material will have a large thermal expansion at high temperatures. The above two factors will reduce the activation energy barrier of cation migration, accelerate the structural transformation, affect the thermal runaway temperature of the battery, and reduce the thermal stability of the battery. In addition, safety problems are not limited to the charging process but may also occur during storage, especially high-temperature storage will increase the safety risks of the battery.^[105]

The thermal stability of high-nickel cathode materials is related to many factors, among which the structure and composition of materials are the most critical factors. Compared with high-nickel materials, low-nickel materials have better thermal stability, so the stability of the anode material can be improved by increasing the content of Mn and reducing the content of Ni. Secondly, the thermal stability of high-nickel ternary materials can also be improved by increasing the grain size and decreasing the specific surface area of cathode particles.

3.2. Modification Strategy of High-Nickel Layered Cathode Material

To solve the above problems, the researchers explored a variety of modification strategies. So far, methods to improve the

inherent defects and electrochemical properties of materials have mainly involved the development of novel synthesis methods, element doping, surface coating, single-crystal structure design, and concentration gradient regulation.

3.2.1. Development of Novel Synthesis Methods

Coprecipitation combined with solid phase sintering reaction is the most mature and traditional method for the preparation of high-nickel cathode materials. Among them, the precise regulation between the reactants as well as the calcination parameters is crucial for the quality of the final product.^[106] However, limited by the reaction conditions, the preparation process inevitably leads to the formation of inherent defects, such as high surface residual lithium content, severe cationic mixing, and oxygen vacancy. Although proper washing or pickling can reduce the side effects of surface residual lithium, improving cationic mixing and crystal structure defects requires more advanced synthesis methods.^[107]

In view of the serious cationic mixing in high-nickel cathode materials, pretreatment with oxidizer or oxygen plasma is one of the effective strategies to improve ion mixing. Xie et al.^[108] improved the $\text{Li}^+/\text{Ni}^{2+}$ mixing of $\text{LiNi}_{0.8}\text{Co}_{0.15}\text{Al}_{0.05}\text{O}_2$ cathode by using a lossless plasma strategy, and improved the cycling performance. The high energy active groups (O_1 , $\cdot\text{OH}$, O_3 , O_3^\bullet) produced by pretreatment can cause $\text{Ni}^{2+} \rightarrow \text{Ni}^{3+}$ oxidation of nickel ions in the cathode. This peroxidation treatment on the surface of

the cathode can effectively slow down the structural transformation in the subsequent synthesis process, thus improving the electrochemical performance of the cathode. In addition, the introduction of a small amount of oxidant (such as $\text{Na}_2\text{S}_2\text{O}_8$, etc.) in the precursor mixing process and subsequent solid-phase sintering can regulate the cation mixing.^[109] Chen et al.^[109] prepared and synthesized the ordered NiOOH layer by $\text{Na}_2\text{S}_2\text{O}_8$ pre-treatment, which effectively reduced $\text{Li}^+/\text{Ni}^{2+}$ mixing and finally improved the cycle stability.

In addition, the introduction of a small amount of oxygen vacancy to the particle surface also helps to improve the degradation of the structure. Wu et al.^[110] used the N_2 atmosphere pre-treatment strategy to construct oxygen vacancy on the surface of the material and thus generate a high-density dislocation layer, effectively slowing down the continuous diffusion of intergranular cracks during the cycle. In addition, hydrothermal synthesis can also be used to prepare stable high-nickel cathode materials to improve the performance of batteries.^[111] However, the process of these new synthesis methods is relatively complex, so it is difficult to achieve large-scale production and application.

3.2.2. Element Doping

Doping of exogenous ions in ternary materials is the most commonly used modification strategy, and it is also one of the effective strategies to reduce the $\text{Li}^+/\text{Ni}^{2+}$ mixing and improve structural stability. According to the type of doped elements, it can be divided into cationic doping and anionic doping. Commonly used cations are Mg^{2+} ,^[98] Zn^{2+} ,^[112] Al^{3+} ,^[113] Zr^{4+} ,^[114] Ti^{4+} , Mo^{6+} , W^{6+} , Nb^{5+} , and Ga^{3+} , which are used to replace some Ni, Co, and Mn positions. In addition, Na^+ with a larger radius can be used to incorporate lithium sites and promote the rapid removal/insertion of lithium ions by widening the diffusion channel of lithium ions. The stability mechanism of cationic doping in the structure is as follows: 1) to reduce the degree of $\text{Li}^+/\text{Ni}^{2+}$ mixing; 2) increase the diffusion coefficient of Li^+ ; 3) slow down the drastic change of lattice parameters; and 4) improve the interface impedance between the electrode and the electrolyte.

Min et al. systematically studied the role of Al and Mg doping in NCM811 system by transmission electron microscopy, DFT, and in situ XRD, and the results showed that the introduction of stable Al–O bond energy can effectively reduce the formation of oxygen vacancies and oxygen precipitation during the cycle. Mg, on the other hand, tends to occupy the Li position, which can reduce the mixing of cations in the highly delithiated state. In situ XRD results show that Mg doping can reduce the dramatic volume change. In addition, doping of high-valence elements induces the formation of Ni^{2+} during the preparation process and causes a small amount of Ni^{2+} to occupy the lithium site. The appropriate amount of Ni^{2+} occupying the lithium site can play the role of “columnar ion” in the lattice, which can enhance the stability of the structure. Wang et al. found a nanoscale cationic disordered phase formed in situ in Ce-doped NCM811 particles. Due to the stable “pillar effect” and the stronger Ce–O bond, the ion migration rate of the modified sample is significantly better than that of the undoped material, and the modification of Ce

also inhibits the formation of the NiO phase. In addition, the proportion of dopants is usually low due to the intrinsic properties of electrochemical inertness. A small amount of dopant will produce heterogeneity in spatial distribution, resulting in differences in electronic structure, crystal structure and microscopic morphology. In order to obtain accurate element distribution, Qian et al.^[114] conducted an in-depth study on the spatial distribution of Zr in Zr-doped $\text{LiNi}_{0.6}\text{Co}_{0.2}\text{Mn}_{0.2}\text{O}_2$ (NMC622) samples. Considering that the introduction of dopants can affect the redox reaction of Ni, the valence state of Ni in Zr-doped NMC622 samples in delithiated state was first investigated by transmitted X-ray with nanometer resolution. Higher valence Ni was observed at the edge of the doped sample, indicating that Zr has a tendency to aggregate. It was then intuitively observed by 3D fluorescence maps that the Zr concentration was higher at the edge of the particles, while the Zr content was lower at the top and bottom of the particles. Since inhomogeneous doping is usually accompanied by lattice distortion, high strains caused by changes in cell volume can be observed in regions with higher Zr concentrations. This strain induces anisotropic impedance during the cycle, resulting in attenuation of electrochemical performance. Shen et al.^[115] investigated a sodium-doped high-nickel low-cobalt lithium-layered oxide cathode material (NCM-Na), which effectively suppressed detrimental phase transitions and $\text{Li}^+/\text{Ni}^{2+}$ mixing by leveraging the role of sodium ions as electromagnetic centers. The experimental results demonstrated that the doped material achieved higher capacity retention and rate capacity under a high voltage of 4.5 V, while also exhibiting superior cycling stability under high-temperature and low-voltage conditions. Sodium doping improves lithium diffusion kinetics and structural stability by increasing the lithium layer spacing and inhibiting transition metal migration. It also reduces electrolyte decomposition and interfacial reactions, thereby enhancing the electrode-electrolyte interfacial stability. DFT calculations further confirm the positive effects of sodium doping in inhibiting Ni migration and increasing the energy barrier. Kim et al.^[116] investigated the effect mechanism of doped Co^{3+} , Fe^{3+} , Al^{3+} , and Ti^{4+} ions on Li/Ni mixing based on the Goodenough–Kanamori–Anderson rule. The electronic configuration of magnetic Ni^{2+} mixed in the Li layer, doped Fe^{3+} and Co^{3+} ions are $t_{2g}^6d_{z2}1d_{x2-y2}1$, $t_{2g}^3d_{z2}1d_{x2-y2}1$, and t_{2g}^6 , respectively. Ni^{2+} and Fe^{3+} have at least one unpaired electron in the 3d orbital while Co^{3+} does not. Hence, Fe^{3+} form a strong 180° super-exchange interaction with Ni^{2+} whereas Co^{3+} forms a 90° super-exchange interaction with Ni^{2+} . It indicates that Ni^{2+} would not be stable after Co doping, unlike Fe doping, resulting in the suppression of Li/Ni mixing in the Ni-rich layered oxides. In addition, substitution of the other nonmagnetic cations, Al^{3+} and Ti^{4+} , into the TM layer in the Ni-rich layered oxides is expected to restrict the 180° super-exchange interaction as they do not have any electrons in their 3d shell. The Li/Ni exchange energy with four different dopants in LiNiO_2 was investigated with DFT calculations, which also supports the above mechanistic reasoning process from another aspect. Huang et al.^[117,118] introduced Ta^{5+} ions into Ni-rich $\text{LiNi}_{0.88}\text{Co}_{0.10}\text{Al}_{0.02}\text{O}_2$ to realize the structure and charge regulation strategy, and the modification strategy was thoroughly investigated. The experimental parameters demonstrate that the regulated surface with partial Ta enrichment

enables high reversibility of Li^+ insertion/extraction by preventing surface Ni reduction in deep charging. Moreover, bulk charge regulation that boosts charge density and its localization on oxygen remarkably suppresses microcracks and oxygen loss, which in turn prevents the fragmentation of the regulated surface and structural degradation associated with oxygen skeleton.

Since primary particles in ternary cathode materials are mostly randomly oriented, the anisotropic lattice volume changes caused by the phase transition result in the formation of microcracks. The formation of microcracks will lead to the erosion of the electrolyte inside the particles, which will aggravate the structural degradation and capacity attenuation. Kim et al. found that Nb doping could change the morphology of primary particles in the cathode of $\text{LiNi}_{0.855}\text{Co}_{0.13}\text{Al}_{0.015}\text{O}_2$ (NCA85). The results show that with the increase of Nb doping, the primary particles of the NCA85 positive electrode gradually show radial arrangement. The radial arrangement of primary particles alleviates the influence of the H2–H3 phase transition in the charging process to a certain extent and reduces the elimination of internal strain, so the cyclic stability of the modified cathode at high temperatures can be significantly improved. Meanwhile, the results show that the formation of microcracks is closely related to the microstructure of particles. Therefore, high-nickel cathode materials with high energy density and long life can be reasonably designed by changing the primary particle morphology. Based on this, Park et al. used B doping to regulate the microstructure of $\text{LiNi}_{0.90}\text{Co}_{0.05}\text{Mn}_{0.05}\text{O}_2$ (B-NCM90) particles and significantly improved the cyclic stability. The results of DFT show that by changing the surface energy of different crystal faces, the radially ordered primary particles are constructed by B introduction, thus alleviating the internal strain generated by the process of lithium removal/insertion. At a high temperature of 55 °C, 1 mol% B-NCM90 showed excellent cyclic stability after 100 cycles, with a capacity retention rate of 91%, while the capacity retention rate of NCM90 was only 76%. $dQ \text{ d}V^{-1}$ and *in situ* XRD results show that NCM90 undergoes a series of phase transitions, in which H2–H3 phase transitions lead to a sharp contraction of lattice parameter c , resulting in mechanical stress generation and deterioration of cyclic properties. In addition, the oxidation peak of H2–H3 of NCM90 decreased significantly during 100 cycles, indicating poor reversibility of its phase transition, which is related to the severe collapse of the material structure caused by mechanical strain. On the contrary, B-NCM90 can still maintain H2–H3 peak intensity, which is consistent with its good cyclic stability. CP-SEM results show that, compared with NCM90 material, there are no obvious microcracks in B-NCM90 material, indicating that adjusting the primary particle morphology by B doping can significantly improve the internal strain caused by H2–H3 phase transition so as to maintain the microstructure integrity of the cathode material during the long cycle process. Park et al. found similar effects in Al^{3+} , Ti^{4+} , Nb^{5+} , Ta^{5+} , W^{6+} , and Mo^{6+} doped with $\text{Li}(\text{Ni}_{0.90}\text{Mn}_{0.10})\text{O}_2$ (NM90). The results show that the transition metal ions with high oxidation state are more conducive to the construction of the radial distribution of the primary particles, which can enhance the structural strength of the secondary particles, reduce the internal resistance, and improve the cyclic stability.

Anion doping is also widely used to modify the structure of high-nickel cathode. Compared with cationic doping, anion doping has the following advantages: 1) the doped anion can replace part of the structure O^{2-} , improve the bond energy between the anion and the transition metal cation, and thus improve the stability of the material structure; 2) the inclusion of cations may aggravate the degree of $\text{Li}^+/\text{Ni}^{2+}$ mixing, while anion doping can effectively improve the disordered occupation between lithium ions and transition metal ions, which is more conducive to the realization of theoretical energy density; 3) cations are difficult to improve the transition metal ion dissolution caused by the electrode–electrolyte side reaction, and the incorporation of F can form fluorine oxide compounds, which can effectively inhibit the generation of HF, and then improve the transition metal ion dissolution. Since the atomic radius of F, S,^[119] and Cl^[120] is similar to O, and it is easy to replace the O site in the structure, it is widely used in anion-doped modification. Kim et al. found that F^- occupying the oxygen site could form a strong M-F bond, thus effectively improving transition metal dissolution and structural stability. Li et al.^[121] found through DFT theoretical calculation and neutron diffraction that F⁻ doping can induce the exchange site of adjacent lithium and nickel atoms, thus generating a locally more stable halogenated octahedral structure, thus improving cycle stability. In addition, due to the charge compensation effect, the replacement of O^{2-} by F^- will lead to a small amount of transition metal ion reduction, and the metal ion of the low state can broaden the lattice parameters of the cathode material because of its larger ionic radius, thus enhancing the ion diffusion coefficient and improving the magnification performance. At the same time, the DFT calculation results show that F⁻ doping will expand the band gap of the cathode material, so excessive F⁻ doping is not conducive to electron transport. Except for F⁻ doping, the electronegativity of Cl⁻ (3.16) is lower than that of F⁻ (4.0) and O²⁻ (3.44), so Cl⁻ substitution of some O sites can reduce the electrostatic repulsion between the O-M-O layers during Li-ion removal/insertion.^[120] However, because the amount of Cl⁻ doping is difficult to control, there are few reports on Cl⁻ as a dopant in the NCM system. Multi-ion doping and negative/cationic codoping are also effective strategies to improve the stability of the structure, which can not only partially replace the TM, Li, and O sites in the structure at the same time but also obtain better electrochemical and thermodynamic properties. However, the interaction between different doping elements is more complex, and its internal mechanism has not been thoroughly explored, so it is still necessary to deeply and systematically explore the synergistic mechanism between multi-ions.

3.2.3. Surface Coating

Although element doping can improve the inherent structural defects of cathode materials, the performance attenuation caused by surface-side reactions (such as HF corrosion and CEI formation) remains unresolved. Surface coating can construct a stable protective layer on the particle surface, which can effectively alleviate the side reaction between electrolyte and electrode, inhibit the dissolution of transition metal, and delay the

structural transformation caused by side reaction.^[122] Generally, surface coating materials need to have antielectrolyte dissolution properties and strong oxidation resistance. Currently, widely studied coating materials include metal oxides (Al_2O_3 ,^[123] TiO_2 ,^[124] MgO ,^[125] etc.), metal fluorides (LiF ,^[126] AlF_3 ,^[127] etc.), phosphates (MnPO_4 ,^[128] AlPO_4 ,^[129] $\text{NaTi}_2(\text{PO}_4)_3$,^[130] etc.), and other inert compounds and carbon-based materials (graphene,^[131] polyaniline,^[132] etc.), lithium compounds(Li_3PO_4 ,^[133] LiNbO_3 ,^[134] Li_2ZrO_3 ,^[135] etc.), and other conductive materials. The mechanism of surface coating can be divided into the following three categories: 1) slow down the serious interface side reaction between electrode and electrolyte, thereby improving the dissolution of positive transition metal ions and lattice oxygen precipitation; 2) slow down the phase transition caused by the Jahn-Teller effect and improve the stability of the material structure; and 3) the conductive surface coating can be used to improve the conductivity of the material and enhance the Li^+ interface transmission rate. The coating effect height of the material depends on the type of coating, thickness, uniformity, and coating conditions. The current coating methods mainly include solid phase/wet mixing, sol-gel, chemical vapor deposition (CVD), pulsed layer deposition (PLD), and atomic layer deposition (ALD).^[136]

Oxide is one of the most typical and earliest coating materials and has been widely used in material surface modification. The results show that most of the oxide coating can improve the stability of the cathode and can effectively reduce the side reaction between the cathode and the electrolyte. Li et al.^[137] introduced a thin amorphous ZnO layer on the surface of $\text{LiNi}_{0.6}\text{Co}_{0.2}\text{Mn}_{0.2}\text{O}_2$ (NMC622). It is found that when ZnO coating layer is 1 wt%, the capacity retention rate of 68% is still displayed after 300 cycles, which is significantly better than the original sample's capacity retention rate of 34%. The improvement in cyclic stability can be attributed to the ZnO coating effectively inhibiting severe interfacial side reactions and reducing interfacial resistance, thus significantly improving cyclic stability. Crystal metal oxides are also used to coat materials except for crystalline metal oxide cladding. Herzog et al.^[138] constructed Al_2O_3 , TiO_2 , and ZrO_2 coating layers on $\text{LiNi}_{0.70}\text{Mn}_{0.15}\text{Co}_{0.15}\text{O}_2$ (NMC701515) by dry method. During the cycle, the metal oxides tend to react with Li ions and form $\text{Li}_x\text{Al}_2\text{O}_3/\text{Li}_x\text{ZrO}_{2+0.5x}/\text{Li}_x\text{TiO}_{2+0.5x}$, thus improving the diffusion kinetics of Li^+ . The corresponding electrochemical properties show that the rate performance and cycle performance of the modified material are improved. However, due to different physical parameters, the improvement of long-cycle stability ($\text{ZrO}_2 < \text{TiO}_2 < \text{Al}_2\text{O}_3$) and rate performance ($\text{TiO}_2 < \text{ZrO}_2 < \text{Al}_2\text{O}_3$) is different. Therefore, the role of the coating layer in the material can be further strengthened through reasonable structural design and parameter optimization. In addition, negative thermal expansion (NTE) material is a new coating material appearing in recent years. The introduction of this material with very low expansion properties in the electrode is conducive to improving the stability of the high-nickel cathode. Bai et al.^[139] first applied a typical NTE material (ZrV_2O_7) to modify the surface of NCM622. The electrochemical performance results showed that after NTE modification, the material still had a capacity retention rate of 71.0% after 500 cycles. DOS calculations of the surface O 2p orbitals show that under the influence of Zr, the DOS of oxygen

drops below -4 eV and becomes inert because the introduction of Zr ions regulates the local electron distribution around the surface oxygen. In contrast, there is unstable oxygen on the surface of the unmodified sample, so it is easy to react with the electrolyte and cause the performance to decay. He et al.^[140] introduced a MgTiO_3 (MTO) coating layer that is extremely coherent to the lattice on the surface of single-crystalline $\text{LiNi}_{0.9}\text{Co}_{0.05}\text{Mn}_{0.05}\text{O}_2$ (SC90). The lattice-coherent between MTO coating and SC90 interface was investigated by first-principles calculations. The stronger interaction between MTO(104)/SC(003) plane (-1.64 J m⁻²) and MTO(101)/SC(101) plane (-1.95 J m⁻²) indicates a good lattice matching between the epitaxial MTO coating and SC90. Finally, the lattice-matched MTO coating layer not only suppresses the interfacial side reactions but also modulates the internal stresses to mitigate the intracrystalline cracks, which ultimately greatly enhances the cycling electrochemical performance of the material. Bai et al.^[141] coating a typical piezoelectric material, the LiTaO_3 (LTO), with a piezoelectric coefficient of 14.6 pC N⁻¹ and ionic conductivity of 10^{-6} to 10^{-5} cm² s⁻¹ on the surface of NCM811, which coupled the relationship between the stress-strain effect of internal Ni-rich cathode and the polarized electric field of piezoelectric material during the charging and discharging process. During the discharge process, the polarized potential was of the same orientation as that of the external electric field, which acted as an accelerator to promote Li^+ diffusion at the electrolyte-cathode interface. Simultaneously, the improved Li^+ kinetics could depress the stress-strain accumulation by lowering the interfacial energy barrier and eventually elevating the electrochemical performances of the Ni-rich cathodes.

Although the electrochemical inert coating can protect the particle interior of the cathode by establishing a physical barrier, its inherent ion insulation seriously hinders the diffusion of lithium ions at the interface, especially at large current, which will lead to lower magnification performance. Therefore, the use of lithium ion conductors as cladding layers can achieve effective physical protection and promote the transport of interfacial ions. Yan et al.^[133] injected Li_3PO_4 into the grain boundary of $\text{LiNi}_{0.76}\text{Mn}_{0.14}\text{Co}_{0.10}\text{O}_2$ (NMC761410) to suppress the capacity and voltage decay problems. First of all, the ALD technology is used to introduce Li_3PO_4 coating layer on the particle surface, and then drive Li_3PO_4 to inject into the intergranular space along the grain boundary of the secondary particles by calcination, which can not only promote the rapid transfer of ions, but also bring no side reactions. The results show that the unmodified cathode produces a large number of grain boundary cracks after cycling, but no obvious cracks are observed in the samples coated with Li_3PO_4 , indicating that the coating of Li_3PO_4 can eliminate the crack diffusion along the grain boundary and improve the laminar-spinel-halite phase transition. The above results effectively reflect that the structural decay and performance deterioration of high-nickel cathode materials can be improved by reasonably designing the coating layer. In addition, coating highly conductive carbon on the surface of the high-nickel cathode can also promote electron transport and improve electrochemical performance. Phattharasupakun et al.^[142] prepared a carbon-coated $\text{LiNi}_{0.8}\text{Mn}_{0.1}\text{Co}_{0.1}\text{O}_2$ (NMC811@C) with a typical core-shell structure using a traditional mechanical fusion

mechanism. Due to the presence of the conductive carbon coating, rapid and uniform phase transitions are observed during the cycle without significant hindrance to the diffusion of Li ions. Moreover, at high operating voltage (>4.0 V), the carbon coating inhibited the OER of the structure. A lithium aluminum oxide (LiAlO_2) coating with Li^+ surface conductivity and high chemical stability has also been widely used in coating strategies for Ni-rich cathode materials. However, it is very difficult to achieve controllable and uniform surface deposition of Al-containing compounds on the surface of the precursors of Ni-rich cathodes since aluminum compounds are prone to self-nucleation reactions in the solution. Using DFT calculations, Jiang et al.^[143] found that oxalate has a stronger and moderate binding strength with Al^{3+} than H_2O . It means that using oxalate as ligands during aluminum coating process can inhibit rapid $\text{Al}(\text{OH})_3$ formation in solution through explosive self-nucleation with OH^- addition, which makes heterogeneous nucleation and precursor surface growth difficult. Furthermore, Al-oxalate coordination compound adsorption on the precursor was more favorable than that of Al- H_2O coordination before the $\text{Al}(\text{OH})_3$ formation. The oxalate-assisted LiAlO_2 coating layer ultimately helped the Ni-rich cathode maintain a 97.4% cycle performance after 100 cycles.

In addition, Xu et al. proposed an innovative strategy for surface modification of high-nickel cathode materials. He used protonated polyaniline (PANI) for mild surface washing of a high-nickel terpolymer ($\text{LiNi}_{0.8}\text{Co}_{0.1}\text{Mn}_{0.1}\text{O}_2$, LNCM). PANI could be coated on the surface during washing and used as a protective layer. The results showed that the material (PW-LNCM) after PANI washing maintained the crystal structure of the original material, while significantly reducing the content of residual lithium compounds on the surface and improving the magnification performance and cycle stability of the material.

3.2.4. Design of Concentration Gradient Structure

In the cycle process, the conventional cladding layer and the main structure have the problem of nonsynchronous shrinkage and expansion, which leads to the existence of pores and finally leads to the stripping of the cladding layer. Moreover, the conventional coating layer has some problems such as insufficient thickness uniformity, which will worsen the long-term cycle stability of the material. The structure design of concentration gradient is one of the effective strategies to improve the cycle stability of cathode materials. The concentration gradient structure mainly includes core-shell structure (Figure 12a), shell concentration gradient (CS, Figure 12b), total concentration gradient (FCG, Figure 12c), and double tilt concentration gradient (TSFCG, Figure 12d). The structural design of concentration gradient generally follows the following principles: 1) high-nickel cathode such as $\text{LiNi}_{0.8}\text{Co}_{0.1}\text{Mn}_{0.1}\text{O}_2$ with high specific capacity is designed as the core, and more stable manganese-rich cathode such as $\text{LiNi}_{x}\text{Co}_{1-2x}\text{Mn}_x\text{O}_2$ ($1/3 \leq x \leq 1/2$) is designed as the shell; 2) the structure inside and outside should have the same crystal structure; and 3) a lower calcination temperature should be used to avoid serious cation diffusion between the core-shell interface. The high-nickel material with high capacity but poor stability

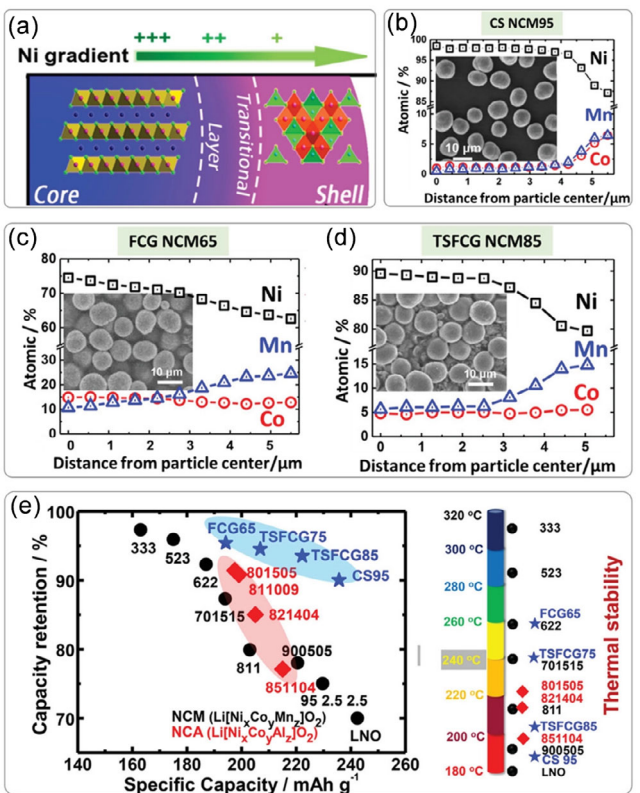


Figure 12. a) Schematic of concentration gradient particles; The concentration gradient of different TM contents in b) CS NCM95, c) FCG NCM65, and d) TSFCG NCM85. e) The relationship between the specific capacity and stability of various layered cathode materials. Reproduced with permission.^[22] Copyright 2021, Wiley-VCH.

located inside the particle, and the manganese rich material with low capacity but good stability is located outside the particle. Among them, the manganese-rich outer region plays the role of a coating layer, which can not only improve the side reaction between the electrode and the electrolyte but also reduce the cost; more importantly, it also has electrochemical activity, so this special structural design can well balance high specific capacity and long cycle stability.

The study of concentration-gradient materials originates from the core-shell structure. Sun et al.^[144] in order to integrate the advantages of $\text{LiNi}_{0.8}\text{Co}_{0.1}\text{Mn}_{0.1}\text{O}_2$ and $\text{LiNi}_{0.5}\text{Mn}_{0.5}\text{O}_2$, $\text{Li}[(\text{Ni}_{0.8}\text{Co}_{0.1}\text{Mn}_{0.1})_{0.8}(\text{Ni}_{0.5}\text{Mn}_{0.5})_{0.2}]\text{O}_2$ core-shell cathode materials were designed and prepared. The structure uses $\text{LiNi}_{0.8}\text{Co}_{0.1}\text{Mn}_{0.1}\text{O}_2$ as the core and $\text{LiNi}_{0.5}\text{Mn}_{0.5}\text{O}_2$ as the shell. It was found that the core provides a high capacity, while the shell enhances the thermal stability of the material and therefore exhibits good cyclic properties. However, in this material, due to the high nickel content of the core during the H2-H3 phase transition process, the volume contraction is more severe than that of the shell, resulting in greater radial stress at the core-shell interface, and eventually, the separation of the two parts of the core-shell. Subsequently, Sun et al.^[145] designed and prepared gradient materials with an average composition of $\text{LiNi}_{0.64}\text{Co}_{0.18}\text{Mn}_{0.18}\text{O}_2$. In this structure, the shell composition was $\text{LiNi}_{0.46}\text{Co}_{0.23}\text{Mn}_{0.31}\text{O}_2$. The transition metal ions are transferred to the core with a higher proportion

of nickel ($\text{LiNi}_{0.8}\text{Co}_{0.1}\text{Mn}_{0.1}\text{O}_2$) in the form of a concentration gradient, which effectively ensures the continuity of the concentration at the junction between the core and the shell and improves the cycle stability. In addition, Sun et al.^[146] found that the primary particle morphology of the shell layer has a great influence on the core–shell gradient material and proved that the use of radially arranged rod-like primary particles in the shell can reduce the stress concentration caused by the anisotropic volume change, thus improving the mechanical strength of the particles and improving the cyclic stability. Recently, Huang et al.^[147] successfully designed and synthesized a concentration-gradient nickel-rich NCM cathode material, $\text{LiNi}_{0.8}\text{Co}_{0.1}\text{Mn}_{0.1}\text{O}_2$ (CG-NCM), via a coprecipitation method. The study demonstrates that CG-NCM delivers a discharge capacity of $\approx 180.1 \text{ mAh g}^{-1}$ at a 1 C rate and retains 96.2% of its initial capacity after 100 cycles, significantly outperforming the conventional C-NCM material. In addition to enhancing chemical stability, the CG-NCM features a unique structural design from a mechanical perspective: its radially aligned nanorod structure and Mn-enriched shell effectively dissipate stress, reduce crack formation, and improve mechanical stability. This dual strategy of enhancing stability from both chemical and mechanical aspects offers new insights for the design of high-performance lithium-ion batteries and propels the development of high-energy-density battery technologies.

Although the core–shell gradient structure can improve the core–shell mismatch, it has a limited effect on stabilizing the surface structure due to the thin thickness of the shell (about 3 μm). Therefore, the researchers designed and developed a full-concentration gradient material (FCG). Sun et al.^[148] synthesized the $\text{LiNi}_{0.75}\text{Co}_{0.10}\text{Mn}_{0.15}\text{O}_2$ cathode material with full concentration gradient for the first time, in which the nickel content gradually decreased from the core to the shell while the manganese concentration gradually increased. Electrochemical test results show that the first cycle discharge capacity up to 215.4 mAh g^{-1} , 100 cycles have a capacity retention rate of 90%. Then, continue to optimize the synthesis of the full concentration gradient material of Al doping $\text{Li}[\text{Ni}_{0.60}\text{Co}_{0.12}\text{Mn}_{0.272}\text{Al}_{0.007}]\text{O}_2$; the material still has 84% of the capacity retention after 3000 cycles.^[149] However, the fundamental mechanism of the nickel concentration gradient's stabilization effect remains elusive because it is inseparable from nickel atomic concentration and nickel-valence gradient effect caused by the cation composition. Yang et al.^[150] design and synthesize a $\text{LiNi}_{0.8}\text{Mn}_{0.1}\text{Co}_{0.1}\text{O}_2$ material that is compositionally uniform and has a hierarchical valence gradient with Ni^{2+} -rich shell, which aims to isolate nickel's valence gradient effect. The results suggest that introducing Ni-valence gradient from the surface to center of the secondary particle of Ni-rich material can effectively stabilize the surface of secondary particles and mitigate the electrochemical performance fading caused by internal structure degradation without sacrificing the capacity.

In order to further develop high-capacity cathode materials, Lim et al.^[151] designed and developed a double inclined concentration gradient material (TSCFG) based on the idea of a full concentration gradient, whose average composition is $\text{Li}[\text{Ni}_{0.65}\text{Co}_{0.13}\text{Mn}_{0.22}]\text{O}_2$. The components of the shell and core are $\text{Li}[\text{Ni}_{0.60}\text{Co}_{0.12}\text{Mn}_{0.28}]\text{O}_2$ and $\text{Li}[\text{Ni}_{0.72}\text{Co}_{0.11}\text{Mn}_{0.17}]\text{O}_2$, respectively. The concentration distribution of Ni and Mn presents

two linear regions with different slopes, in which the concentration of nickel decreases slowly at the core and increases near the surface. This design achieves a higher Ni proportion of the core, which has a higher discharge capacity, and can guarantee a higher Mn concentration of the shell for a more stable external structure. Compared with traditional high-nickel ternary materials, the concentration gradient materials have greater advantages. On the one hand, due to the lower nickel content on the surface of the material, the interface side reaction between the electrode/electrolyte is improved. On the other hand, due to the high consistency of grain orientation in gradient materials, the anisotropic volume strain caused by lithium-ion removal/incarceration can be dissipated, which inhibits the formation and diffusion of microcracks, thus ensuring the integrity of the microstructure and improving the cyclic stability.^[152] However, there are some difficulties in the preparation of concentration gradient materials. First, the synthesis process of concentration gradient precursors requires accurate and fine regulation of coprecipitation parameters, especially pH, chelating agent concentration, and transition metal ion solution addition ratio. In addition, it is difficult to control the diffusion of transition metal ions in the bulk phase during high-temperature solid phase reactions. Therefore, high-nickel cathode materials with concentration gradients are still difficult to produce commercially.

3.2.5. Single-Crystal Material Design

As mentioned above, in the charge and discharge process of polycrystalline cathode materials, the $\text{H}_2 \rightarrow \text{H}_3$ phase transition will produce anisotropic nonuniform stress and concentrate at the grain boundary. The concentration of local stress leads to the formation of intergranular cracks, which leads to more serious side reactions at the electrode–electrolyte interface, and then induces the dissolution, migration, and segregation of transition metal ions (TMs) and structural reconstruction. This results in an increase in impedance and deterioration of battery performance. In addition, the electrode rolling process can lead to the breakdown of secondary particles, thus destroying the integrity of the microstructure and leading to deterioration of performance. In order to solve these problems, the ideal method is to control the morphology to prevent structural damage and the generation and diffusion of intergranular cracks. Compared with traditional polycrystalline particles, single-crystal cathode particles have high crystallinity and isotropy, so they can slow down the formation of grain boundary cracks during high-pressure compaction and charge-discharge process, enhance the interface stability and reduce oxygen precipitation, and maintain the integrity of the microstructure and crystal structure, thus improving the cyclic stability of the positive electrode and enhancing the safety performance.

However, compared with polycrystalline cathode materials, the preparation of single-crystal cathode materials is more difficult, and the synthesis methods mainly include high-temperature calcination, step-by-step calcination, and molten salt method. The sintering temperature is one of the key factors in controlling the solid lithium reaction. Increasing the sintering temperature

can promote the diffusion rate of ions and accelerate the growth of grains so that the particles with single-crystal morphology can be obtained. Wang et al.^[153] systematically studied the solid-phase sintering process, and the results showed that with the increase in calcination time, the larger the grain size of the cathode of $\text{LiNi}_{0.8}\text{Co}_{0.15}\text{Al}_{0.05}\text{O}_2$, the higher the agglomeration degree. In situ XRD and SEM measurements show that the crystallinity of the monocrystal materials formed after sintering for 5 h is better. Compared with the polycrystalline cathode, the monocrystalline cathode exhibits better cyclic stability. However, the preparation of single crystals usually requires additional mechanical forces to disperse the particles, which leads to the fracture of the particles and the formation of fine powders, thus intensifying the surface restructuring (lamellar phase → spinel phase → halite phase). In addition, high-temperature calcination will also increase the degree of Li/Ni ion mixing. Therefore, single-crystal cathode materials prepared at high temperatures require additional annealing procedures to repair their structural defects. Huang et al.^[154] systematically studied the morphological differences of NCM622 single-crystal particles before and after annealing, and the results showed that the broken particles could be refused by annealing treatment, making the surface smoother, and the electrochemical performance was also improved after annealing treatment. In addition, multistep calcination can well balance the morphology of single-crystal materials and crystal structure, prepare particles with uniform particle size distribution, and ensure that they have a low cationic mixing degree. Li et al.^[155] successfully synthesized single-crystal cathode materials such as $\text{LiNi}_{0.88}\text{Co}_{0.09}\text{Al}_{0.03}\text{O}_2$, $\text{LiNi}_{0.95}\text{Al}_{0.05}\text{O}_2$, and $\text{LiNi}_{0.975}\text{Mg}_{0.025}\text{O}_2$.

Partial LiOH ($\text{Li}/\text{TM} = 0.9$) was added during the first calcination process, and the morphology of the material was optimized by high-temperature calcination (850–900 °C). In the second calcination process, the remaining lithium salt is added and the crystal structure of the material is repaired by low-temperature calcination (700–750 °C). In addition, the study also demonstrated that Li/TM and sintering temperature are extremely important for the morphology and properties of single-crystal materials.

The molten salt method is to add an appropriate amount of molten salt at the high-temperature sintering stage so as to promote the growth of grain at a lower temperature. This is because molten salt has the properties of solution at high temperature, which can provide more paths for crystal growth, and then promote continuous dissolution and recrystallization of products, thereby reducing the calcination temperature of single-crystal preparation, thus reducing $\text{Li}^+/\text{Ni}^{2+}$ mixing and inhibiting particle agglomeration. The commonly used molten salts are mainly NaCl, KCl, LiCl, Li_2SO_4 , LiNO_3 , and ammonium molybdate. Kim et al.^[156] synthesized single-crystal NCM811 by NaCl and KCl molten salt. The results show that NaCl molten salts promote the growth of (003), (104), and (111) crystal faces and show a standard octahedral shape, while the particles synthesized with KCl molten salts show more isotropic shapes. The results of electrochemical performance show that the samples synthesized with NaCl have more discharge capacity than those synthesized with KCl. The oxygen release of the two monocrystalline samples is lower than that of the polycrystalline samples. However, the molten salt process not only requires more raw material costs but also requires subsequent washing treatment to eliminate the residual

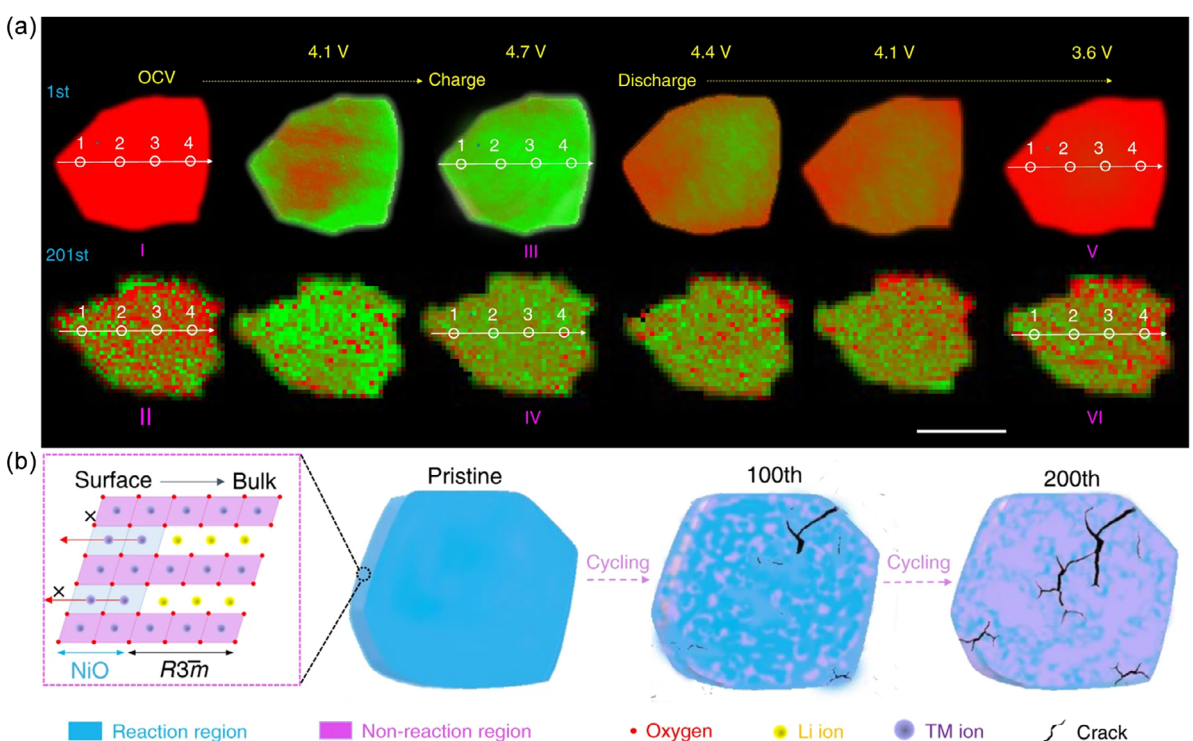


Figure 13. a) Operando 2D chemical phase mapping of the Ni k-edge for NCM particles in the initial and 201st cycles. b) The mechanism of structural degradation of single-crystal NCM. Reproduced with permission.^[167] Copyright 2020, Nature Communications.

cosolvent. Due to the high reactivity of high-nickel materials, Li^+ /H⁺ exchange is easy to occur in the washing process, which will destroy the surface structure of the material and cause the loss of active lithium. Therefore, the selection and ratio of molten salt and the subsequent washing process need to be comprehensively considered.

Manthiram et al.^[157] systematically compared the reaction mechanism of high-temperature calcination and molten salt method. For high-temperature calcination, grain growth at high temperatures mainly depends on grain boundary migration, and there is an exponential relationship between grain boundary migration and temperature. Therefore, the effect of sintering temperature on the growth of single-crystal particles is greater than that of sintering time. In the molten salt process, the growth of grains is dominated by the solution-recrystallization mechanism, and the grains can grow at a faster rate in the two-phase system, thus achieving the growth of micron particles at a lower temperature. However, no matter what kind of single-crystal preparation process is used, the preparation of single-crystal materials has some problems, such as complicated processes and difficult-to-control reaction parameters. At the same time, although the particle structure of a single crystal inhibits the generation of intergranular cracks, the grain size of the micron level produces a long Li⁺ diffusion path, resulting in slow Li⁺ diffusion kinetics. The slow kinetics results in an uneven distribution of lithium

concentration within the single-crystal particles during the cycle, which induces uneven internal stress and plane slip along the (003) crystal face (Figure 13a). This slippage causes the formation of intrasubstalline cracks during the long cycle, ultimately leading to severe surface/interface degradation and capacity decay (Figure 13b).^[158]

3.2.6. The Application of Ni-Rich Cathodes on All-Solid-State Battery

The drive toward Ni-rich NCM has been to augment battery capacity, life cycles, and safety, yet it is severely limited by the traditional liquid electrolytes. All-solid-state batteries (ASSBs) stand out for their inherent safety and the fact that lithium metal can be used as an anode material, which lays the groundwork for significantly enhanced battery capacities. Despite their promise, these technologies face significant interface challenges, notably poor contact and low ion transport efficiency with Ni-rich cathodes, leading to substantial stability issues. During charging and discharging process, the interfacial conductivity between the solid electrolyte and the Ni-rich cathodes decreases dramatically due to the loss of interfacial contact and the increase of diffusion barrier. In addition, anisotropic shrinkage and expansion and inter/intragranular cracks of Ni-rich cathodes also create voids at the solid electrolyte-electrode interface.

Table 1. Comparison of capacity retention rate and periodic performance of different modification policies.

Modification strategies		Retention [%]	Rate [C]	Cycles	References
Development of novel synthesis methods	Plasma treatment	81.2	1	200	[108]
	A facile preoxidation method with a Na ₂ S ₂ O ₈ aqueous solution	89.2	1	100	[109]
	N ₂ annealing treatment	84.41	0.2	100	[110]
Element doping	A urea-based hydrothermal method	92.6	–	50	[111]
	Nanowelding Strategy	96.27	1	100	[120]
	Nb doping	97.1	0.1	100	[140]
	B doping	91	0.5	100	[121]
Surface coating	F doping	96.5	0.5	100	[123]
	ZnO	68	0.2	300	[145]
	Al ₂ O ₃	94.6	0.5	100	[146]
	TiO ₂	86.9	0.5	100	[146]
	ZrO ₂	84.6	0.5	100	[146]
	NTE material (ZrV ₂ O ₇)	66.6	0.2	200	[147]
Design of concentration gradient structure	Carbon	78	1	200	[148]
	Li[(Ni _{0.8} Co _{0.1} Mn _{0.1}) _{0.8} (Ni _{0.5} Mn _{0.5}) _{0.2}]O ₂ core–shell cathode materials	98	1	500	[151]
	Li[Ni _{0.64} Co _{0.18} Mn _{0.18}]O ₂ material with concentration gradient structure	96	0.5	50	[152]
	Li[Ni _{0.60} Co _{0.15} Mn _{0.25}]O ₂ with the nanorod shell	85.5	0.5	150	[153]
	LiNi _{0.75} Co _{0.10} Mn _{0.15} O ₂ cathode material with full concentration gradient	90	1	100	[155]
Single-crystal material design	the full concentration gradient material of Al doping	84.5	1	3000	[156]
	Li[Ni _{0.600} Co _{0.121} Mn _{0.272} Al _{0.007}]O ₂	96.6	0.5	100	[157]
	Li[Ni _{0.65} Co _{0.13} Mn _{0.22}]O ₂ with two-slope full concentration gradient	88	1	200	[167]
	Single-crystal LiNi _{0.8} Co _{0.15} Al _{0.05} O ₂ (SC-NCA)	94.7	–	50	[160]
	LiNi _{0.6} Mn _{0.2} Co _{0.2} O ₂ (SC622)	98.7	1	100	[162]

Specially, liquid electrolytes can penetrate into polycrystalline Ni-rich cathode intergranular cracks to promote Li⁺ diffusion, but the mechanical rigidity of solid-state electrolytes means that such cracks impede Li⁺ diffusion. Sun et al.^[159] quantified the capacity fading factors of Ni-rich LiNi_xCo_yAl_{1-x-y}O₂ composite ASSB cathodes as functions of Ni content. Surface degradation at the cathode–electrolyte interface was found to be the main cause of capacity fading in a Ni-rich cathodes with 80% Ni content, whereas inner-particle isolation and detachment of the Ni-rich cathodes from the electrolyte play a substantial role as the Ni content increases to 85% or more. Sun et al.^[160] simultaneously applied single/polycrystalline LiNi_{0.5}Mn_{0.3}Co_{0.2}O₂ to solid-state electrolytes and found that the single-crystalline material exhibits 6–14 times higher Li⁺ diffusion coefficient than polycrystalline LiNi_{0.5}Mn_{0.3}Co_{0.2}O₂. Single crystals, with fewer grain boundaries than polycrystals, facilitate smoother Li⁺ transport, effectively prevent particle fragmentation, and widely study for solid-state electrolyte applications.

Currently the solid electrolytes matched with high-nickel ternary cathodes are generally inorganic, such as, Li₁₀SnP₂S₁₂,^[161] Li₂TaCl₇,^[162] and organic polymers.^[163,164] Inorganic-based solid-state electrolytes tend to have high Li-ion conductivity due to the efficient ion channels and low activation energy transport mechanisms in their crystals, but the rigid material properties make the high interfacial impedance at the electrolyte/electrode interface still a serious problem. In contrast, organic-like solid electrolytes with flexibility can be well adhered to the cathode material during charging-discharging process. However, limited by polymer chain dynamics and carrier-coupled transport, organic-based electrolytes have low internal lithium ion conductivity (**Table 1**).

4. Conclusion and Outlook

High-nickel layered cathode material is an ideal choice for lithium-ion battery cathode materials due to its high energy density and relatively low cost. However, there are some inherent defects in the material itself that affect its further large-scale application. First of all, the high-nickel layered cathode materials face structural defects such as cationic ion mixing and oxygen vacancy during the preparation process. And the surface residual lithium prevalent in high nickel will not only increase the difficulty of electrode preparation but also lead to subsequent serious battery gas production and cause safety problems. Secondly, ion migration and dissolution, interfacial side reactions, microcracks, and irreversible structural transformation during the cycle lead to sharp capacity attenuation. Although the monocrystalline structure can improve the mechanical instability and other problems, it has its own problems such as slow lithium ion diffusion dynamics, crystal surface slip, intracrystalline cracks, and volume phase reaction heterogeneity. Therefore, it is necessary to develop reasonable modification strategies, such as regulating the composition and microstructure, surface interface modification, and ion doping, to improve the stability of the crystal structure and surface interface of the material, inhibit the interface side reaction between the electrode and the electrolyte, and maintain the

integrity of the microstructure, so as to realize the large-scale application of high-nickel/ultrahigh-nickel polycrystalline/single-crystal cathode materials. Specifically, work can be carried out from the following aspects:

1. The influence of grain structure and grain boundary on the homogeneity and reversibility of electrochemical reaction of cathode materials was revealed by *in situ* technique;
2. Regulate the generation and diffusion of oxygen vacancies in the bulk phase and improve the irreversible oxygen loss of the lattice and the heat and gas production of the battery;
3. To develop a stable and feasible single-crystal ultrahigh-nickel cathode material and to optimize the grain structure in one step by theoretical calculation so as to improve the heterogeneity of bulk reaction;
4. Combined with solid electrolyte technology to develop lithium-ion batteries with better safety.

Acknowledgements

This work was supported by the project from the National Natural Science Foundation of China [U20A20145]; Ordos “Open bidding for selecting the best candidates” program (JBGS-2023-004); State Key Laboratory of Polymer Materials Engineering [no. sklpme2020-3-02], Sichuan Provincial Department of Science and Technology [no. 2020YFG0022; no. 2022YFG0124], Dazhou Department of Science and Technology [no. 21ZDYF0001], Guangyuan Department of Science and Technology [no. 22ZDYF0047], Sichuan Province Science and Technology Achievement Transfer and Transformation Project [no. 21ZHSF0111], 2020 Strategic Cooperation Project between Sichuan University and Suining Municipal People’s Government [no. CDSN-02]; and the 2023 Strategic Cooperation Project between Sichuan University and Zigong Municipal People’s Government [no. 2023CDZG-01].

Conflict of Interest

The authors declare no conflict of interest.

Keywords: high-nickel • lithium-ion batteries • modification strategies

- [1] H. Yang, D. Wang, Y. Liu, Y. Liu, B. Zhong, Y. Song, Q. Kong, Z. Wu, X. Guo, *Energy Environ. Sci.* **2024**, *17*, 1756.
- [2] S. Ramachandran, U. Stimming, *Energy Environ. Sci.* **2015**, *8*, 3313.
- [3] L. Zhou, K. Zhang, Z. Hu, Z. Tao, L. Mai, Y.-M. Kang, S. L. Chou, J. Chen, *Adv. Energy Mater.* **2018**, *8*, e1701415.
- [4] F. Yang, Y. Xie, Y. Deng, C. Yuan, *Nat. Commun.* **2018**, *9*, 2429.
- [5] D. Chen, W. Zhang, K. Luo, Y. Song, Y. Zhong, Y. Liu, G. Wang, B. Zhong, Z. Wu, X. Guo, *Energy Environ. Sci.* **2021**, *14*, 2244.
- [6] Y. Xiao, N. M. Abbasi, Y. F. Zhu, S. Li, S. J. Tan, W. Ling, L. Peng, T. Yang, L. Wang, X. D. Guo, Y. X. Yin, H. Zhang, Y. G. Guo, *Adv. Funct. Mater.* **2020**, *30*, 2001334.
- [7] M. E. Weeks, M. E. Larson, *J. Chem. Educ.* **1937**, *14*, 403.
- [8] W. S. Harris, *Electrochemical Studies in Cyclic Esters*, University of California Radiation Laboratory, Berkeley, 1958.
- [9] S. Ghosh, U. Bhattacharjee, S. Bhowmik, S. K. Martha, *J. Energy Power Technol.* **2022**, *1*, 002.
- [10] F. R. Gamble, J. H. Osiecki, M. Cais, R. Pisharody, F. J. DiSalvo, T. H. Geballe, *Science* **1971**, *174*, 493.

- [11] G. V. S. Rao, J. C. Tsang, *Mater. Res. Bull.* **1974**, *9*, 921.
- [12] M. S. Whittingham, *Science* **1976**, *192*, 1126.
- [13] N. A. Godshall, I. D. Raistrick, R. A. Huggins, *Mater. Res. Bull.* **1980**, *15*, 561.
- [14] K. Mizushima, P. C. Jones, P. J. Wiseman, J. B. Goodenough, *Mater. Res. Bull.* **1980**, *15*, 783.
- [15] M. Zanini, S. Basu, J. E. Fischer, *Carbon* **1978**, *16*, 211.
- [16] R. Yazami, P. Touzain, *J. Power Sources* **1983**, *9*, 365.
- [17] R. Fong, U. Vonsacken, J. R. Dahn, *J. Electrochem. Soc.* **1990**, *137*, 2009.
- [18] M. Li, J. Lu, Z. Chen, K. Amine, *Adv. Mater.* **2018**, *30*, 1800561.
- [19] A. K. Padhi, K. S. Nanjundaswamy, J. B. Goodenough, *J. Electrochem. Soc.* **1997**, *144*, 1188.
- [20] M. M. Thackeray, S. H. Kang, C. S. Johnson, J. T. Vaughey, R. Benedek, S. A. Hackney, *J. Mater. Chem.* **2007**, *17*, 3112.
- [21] C. X. Zu, H. Li, *Energy Environ. Sci.* **2011**, *4*, 2614.
- [22] M. Jiang, D. L. Danilov, R.-A. Eichel, P. H. L. Notten, *Adv. Energy Mater.* **2021**, *11*, 2103005.
- [23] Z. Z. Cui, X. Li, X. Y. Bai, X. D. Ren, X. Ou, *Energy Storage Mater.* **2023**, *57*, 14.
- [24] A. Manthiram, *Nat. Commun.* **2020**, *11*, 1550.
- [25] M. Nishizawa, S. Yamamura, T. I. Uchida, *Chem. Commun.* **1998**, 1631.
- [26] R. V. Chebiam, F. Prado, A. Manthiram, *Chem. Mater.* **2001**, *13*, 2951.
- [27] R. V. Chebiam, A. M. Kannan, F. Prado, A. Manthiram, *Electrochem. Commun.* **2001**, *3*, 624.
- [28] X. Lu, Y. Sun, Z. Jian, X. He, L. Gu, Y. S. Hu, H. Li, Z. Wang, W. Chen, X. Duan, L. Chen, J. Maier, S. Tsukimoto, Y. Ikuhara, *Nano Lett.* **2012**, *12*, 6192.
- [29] J. N. Zhang, Q. Li, C. Ouyang, X. Yu, M. Ge, X. Huang, E. Hu, C. Ma, S. Li, R. Xiao, W. Yang, Y. Chu, Y. Liu, H. Yu, X. Q. Yang, X. Huang, L. Chen, H. Li, *Nat. Energy* **2019**, *4*, 594.
- [30] M. D. Radin, S. Hy, M. Sina, C. Fang, H. Liu, J. Vinckeviciute, M. Zhang, M. S. Whittingham, Y. S. Meng, A. Van der Ven, *Adv. Energy Mater.* **2017**, *7*, 160288.
- [31] A. W. Golubkov, R. Planteu, P. Krohn, B. Rasch, B. Brunnsteiner, A. Thaler, V. Hacker, *RSC Adv.* **2018**, *8*, 40172.
- [32] N. Muralidharan, E. C. Self, M. Dixit, Z. Du, R. Essehlri, R. Amin, J. Nanda, I. Belharouak, *Adv. Energy Mater.* **2022**, *12*, 33.
- [33] A. Manthiram, A. V. Murugan, A. Sarkar, T. Muraliganth, *Energy Environ. Sci.* **2008**, *1*, 621.
- [34] D. H. Cho, C. H. Jo, W. Cho, Y. J. Kim, H. Yashiro, Y. K. Sun, S. T. Myung, *J. Electrochem. Soc.* **2014**, *161*, A920.
- [35] M. Bianchini, M. Roca-Ayats, P. Hartmann, T. Brezesinski, J. Janek, *Angew. Chem. Int. Ed.* **2019**, *58*, 10434.
- [36] J. C. Hunter, *J. Solid State Chem.* **1981**, *39*, 142.
- [37] C. Zhan, J. Lu, A. J. Kropf, T. Wu, A. N. Jansen, Y.-K. Sun, X. Qiu, K. Amine, *Nat. Commun.* **2013**, *4*, 2437.
- [38] W. E. Gent, G. M. Busse, K. Z. House, *Nat. Energy* **2022**, *7*, 1132.
- [39] X. Wang, Y.-L. Ding, Y.-P. Deng, Z. Chen, *Adv. Energy Mater.* **2020**, *10*, 1903864.
- [40] K. Luo, M. R. Roberts, R. Hao, N. Guerrini, D. M. Pickup, Y.-S. Liu, K. Edström, J. Guo, A. V. Chadwick, L. C. Duda, P. G. Bruce, *Nat. Chem.* **2016**, *8*, 684.
- [41] M. D. Radin, J. Vinckeviciute, R. Seshadri, A. Van der Ven, *Nat. Energy* **2019**, *4*, 639.
- [42] G. Assat, J. M. Tarascon, *Nat. Energy* **2018**, *3*, 373.
- [43] D. H. Seo, J. Lee, A. Urban, R. Malik, S. Kang, G. Ceder, *Nat. Chem.* **2016**, *8*, 692.
- [44] M. M. Thackeray, W. I. F. David, P. G. Bruce, J. B. Goodenough, *Mater. Res. Bull.* **1983**, *18*, 461.
- [45] M. M. Thackeray, *J. Electrochem. Soc.* **1995**, *142*, 2558.
- [46] W. Choi, A. Manthiram, *J. Electrochem. Soc.* **2006**, *153*, A1760.
- [47] A. Manthiram, K. Chemelewski, E. S. Lee, *Energy Environ. Sci.* **2014**, *7*, 1339.
- [48] J. Lee, D. A. Kitchae, D. H. Kwon, C. W. Lee, J. K. Papp, Y. S. Liu, Z. Lun, R. J. Clément, T. Shi, B. D. McCloskey, J. Guo, M. Balasubramanian, G. Ceder, *Nature* **2018**, *556*, 185.
- [49] J. Lee, D. H. Seo, M. Balasubramanian, N. Twu, X. Li, G. Ceder, *Energy Environ. Sci.* **2015**, *8*, 3255.
- [50] J. Lee, A. Urban, X. Li, D. Su, G. Hautier, G. Ceder, *Science* **2014**, *343*, 519.
- [51] W. Lee, S. Muhammad, S. Chernov, H. Lee, J. Yoon, Y. M. Kang, W. S. Yoon, *Angew. Chem. Int. Ed.* **2020**, *59*, 2578.
- [52] Z. L. Liu, A. S. Yu, J. Y. Lee, *J. Power Sources* **1999**, *81*, 416.
- [53] M. Yoshio, H. Noguchi, J. Itoh, M. Okada, T. Mouri, *J. Power Sources* **2000**, *90*, 176.
- [54] T. Ohzuku, Y. Makimura, *Chem. Lett.* **2001**, *30*, 642.
- [55] P. Y. Liao, J. G. Duh, S. R. Sheen, *J. Electrochem. Soc.* **2005**, *152*, A1695.
- [56] M. H. Kim, H. S. Shin, D. Shin, Y. K. Sun, *J. Power Sources* **2006**, *159*, 1328.
- [57] J. Li, L. Wang, Q. Zhang, X. He, *J. Power Sources* **2009**, *189*, 28.
- [58] H. J. Noh, S. Youn, C. S. Yoon, Y. K. Sun, *J. Power Sources* **2013**, *233*, 121.
- [59] W. Liu, P. Oh, X. Liu, M. J. Lee, W. Cho, S. Chae, Y. Kim, J. Cho, *Angew. Chem. Int. Ed.* **2015**, *54*, 4440.
- [60] D. S. Ko, J. H. Park, S. Park, Y. N. Ham, S. J. Ahn, J. H. Park, H. N. Han, E. Lee, W. S. Jeon, C. Jung, *Nano Energy* **2019**, *56*, 434.
- [61] A. Aishova, G.-T. Park, C. S. Yoon, Y.-K. Sun, *Adv. Energy Mater.* **2020**, *10*, 1903179.
- [62] U. H. Kim, L. Y. Kuo, P. Kagazchi, C. S. Yoon, Y. K. Sun, *ACS Energy Lett.* **2019**, *4*, 576.
- [63] H. Huang, L. Zhang, H. Tian, J. Yan, J. Tong, X. Liu, H. Zhang, H. Huang, S. Hao, J. Gao, L. Yu, H. Li, J. Qiu, W. Zhou, *Adv. Energy Mater.* **2023**, *13*, 2203188.
- [64] L. Song, M. Xiao, J. Du, L. Li, T. Zhao, Y. Xia, Y. Xiang, T. Chen, L. Jiang, Z. Xiao, Q. Yan, X. Peng, *J. Energy Storage* **2024**, *98*, 113123.
- [65] Y. F. Su, L. W. Li, G. Chen, L. Chen, N. Li, Y. Lu, L. Y. Bao, S. Chen, F. Wu, *Chin. J. Chem.* **2021**, *39*, 189.
- [66] A. C. Martinez, S. Grugeon, D. Cailleau, M. Courty, P. Tran-Van, B. Delobel, S. Laruelle, *J. Power Sources* **2020**, *468*, 228204.
- [67] I. A. Shkrob, J. A. Gilbert, P. J. Phillips, R. Klie, R. T. Haasch, J. Bareño, D. P. Abraham, *J. Electrochem. Soc.* **2017**, *164*, A1489.
- [68] T. Toma, R. Maezono, K. Hongo, *ACS Appl. Energy Mater.* **2020**, *3*, 4078.
- [69] A. Butt, G. Ali, K. T. Kubra, R. Sharif, A. Salman, M. Bashir, S. Jamil, *Energy Technol.* **2022**, *10*, 2100775.
- [70] Y. Kim, *J. Mater. Sci.* **2013**, *48*, 8547.
- [71] Y. Kim, *Phys. Chem. Chem. Phys.* **2013**, *15*, 6400.
- [72] X. H. Xiong, Z. X. Wang, P. Yue, H. Guo, F. Wu, J. Wang, X. Li, *J. Power Sources* **2013**, *222*, 318.
- [73] C. H. Jo, D. H. Cho, H. J. Noh, H. Yashiro, Y. K. Sun, S. T. Myung, *Nano Res.* **2015**, *8*, 1464.
- [74] U. H. Kim, D. W. Jun, K. J. Park, Q. Zhang, P. Kagazchi, D. Aurbach, D. T. Major, G. Goobes, M. Dixit, N. Leifer, C. M. Wang, P. Yan, D. Ahn, K. H. Kim, C. S. Yoon, Y. K. Sun, *Energy Environ. Sci.* **2018**, *11*, 1271.
- [75] J. R. Dahn, U. Vonsacken, M. A. Michal, *Solid State Ionics* **1990**, *44*, 87.
- [76] Y. Xiao, T. Liu, J. Liu, L. He, J. Chen, J. Zhang, P. Luo, H. Lu, R. Wang, W. Zhu, Z. Hu, G. Teng, C. Xin, J. Zheng, T. Liang, F. Wang, Y. Chen, Q. Huang, F. Pan, H. Chen, *Nano Energy* **2018**, *49*, 77.
- [77] E. J. Wu, P. D. Tepeš, G. Ceder, *Philos. Mag. B* **1998**, *77*, 1039.
- [78] J. Zheng, G. Teng, C. Xin, Z. Zhuo, J. Liu, Q. Li, Z. Hu, M. Xu, S. Yan, W. Yang, F. Pan, *J. Phys. Chem. Lett.* **2017**, *8*, 5537.
- [79] D. Wang, C. Xin, M. Zhang, J. Bai, J. Zheng, R. Kou, J. Y. Peter Ko, A. Huq, G. Zhong, C. J. Sun, Y. Yang, Z. Chen, Y. Xiao, K. Amine, F. Pan, F. Wang, *Chem. Mater.* **2019**, *31*, 2731.
- [80] E. Flores, N. Vonruti, P. Novak, U. Aschner, E. J. Berg, *Chem. Mater.* **2018**, *30*, 4694.
- [81] J. Wandt, A. T. S. Freiberg, A. Ogrodnik, H. A. Gasteiger, *Mater. Today* **2018**, *21*, 825.
- [82] S. S. Zhang, *J. Energy Chem.* **2020**, *41*, 135.
- [83] S. E. Renfrew, L. A. Kaufman, B. D. McCloskey, *ACS Appl. Mater. Interfaces* **2019**, *11*, 34913.
- [84] P. Teichert, G. G. Eshetu, H. Jahnke, E. Figgemeier, *Batteries* **2020**, *6*, 8.
- [85] L. Liu, M. Li, L. Chu, B. Jiang, R. Lin, X. Zhu, G. Cao, *Prog. Mater. Sci.* **2020**, *111*, 100655.
- [86] N. Y. Kim, T. Yim, J. H. Song, J. S. Yu, Z. Lee, *J. Power Sources* **2016**, *307*, 641.
- [87] A. T. S. Freiberg, M. K. Roos, J. Wandt, R. de Vivie-Riedle, H. A. Gasteiger, *J. Phys. Chem. A* **2018**, *122*, 8828.
- [88] R. Jung, M. Metzger, F. Maglia, C. Stinner, H. A. Gasteiger, *J. Phys. Chem. Lett.* **2017**, *8*, 4820.
- [89] S. Solchenbach, M. Metzger, M. Egawa, H. Beyer, H. A. Gasteiger, *J. Electrochem. Soc.* **2018**, *165*, A3022.
- [90] S. S. Zhang, *J. Electrochem. Soc.* **2020**, *167*, 100510.
- [91] X. Z. Zhang, C. H. Wan, X. L. Gao, J. M. Wang, X. Y. Tan, *Nature* **2013**, *501*, E1.
- [92] J. Vetter, P. Novák, M. R. Wagner, C. Veit, K. C. Möller, J. O. Besenhard, M. Winter, M. Wohlfahrt Mehrens, C. Vogler, A. Hammouche, *J. Power Sources* **2005**, *147*, 269.
- [93] J. Liu, J. Wang, Y. Ni, K. Zhang, F. Cheng, J. Chen, *Mater. Today* **2021**, *43*, 132.
- [94] S. Watanabe, M. Kinoshita, T. Hosokawa, K. Morigaki, K. Nakura, *J. Power Sources* **2014**, *258*, 210.
- [95] S. Watanabe, M. Kinoshita, K. Nakura, *J. Power Sources* **2014**, *247*, 412.
- [96] C. Xu, P. J. Reeves, Q. Jacquet, C. P. Grey, *Adv. Energy Mater.* **2021**, *11*, 2003404.
- [97] L. de Biasi, A. Schiele, M. Roca-Ayats, G. Garcia, T. Brezesinski, P. Hartmann, J. Janek, *ChemSusChem* **2019**, *12*, 2240.
- [98] Q. Xie, W. Li, A. Manthiram, *Chem. Mater.* **2019**, *31*, 938.
- [99] Z. Ren, C. Shen, M. Liu, J. Liu, S. Zhang, G. Yang, L. Huai, X. Liu, D. Wang, H. Li, *Energy Storage Mater.* **2020**, *28*, 1.
- [100] J. Li, Q. Zhang, X. Xiao, Y. T. Cheng, C. Liang, N. J. Dudney, *J. Am. Chem. Soc.* **2015**, *137*, 13732.

- [101] H. H. Ryu, G. T. Park, C. S. Yoon, Y. K. Sun, *Small* **2018**, *14*, 1803179.
- [102] J. Duan, X. Tang, H. Dai, Y. Yang, W. Wu, X. Wei, Y. Huang, *Electrochim. Energy Rev.* **2020**, *3*, 1.
- [103] M. Dixit, B. Markovsky, F. Schipper, D. Aurbach, D. T. Major, *J. Phys. Chem. C* **2017**, *121*, 22628.
- [104] E. Lee, S. Muhammad, T. Kim, H. Kim, W. Lee, W. S. Yoon, *Adv. Sci.* **2020**, *7*, 1902413.
- [105] S. M. Bak, E. Hu, Y. Zhou, X. Yu, S. D. Senanayake, S. J. Cho, K. B. Kim, K. Y. Chung, X. Q. Yang, K. W. Nam, *ACS Appl. Mater. Interfaces* **2014**, *6*, 22594.
- [106] M. Wood, J. Li, R. E. Ruther, Z. Du, E. C. Self, H. M. Meyer, C. Daniel, I. Belharouak, D. L. Wood, *Energy Storage Mater.* **2020**, *24*, 188.
- [107] Y. F. Su, G. Chen, L. Chen, L. Wei Li, C. Li, R. Ding, J. H. Liu, Z. Lv, Y. Lu, L. Y. Bao, G. Q. Tan, S. Chen, F. Wu, *Front. Chem.* **2020**, *8*, 573.
- [108] K. Yuan, N. Li, R. Ning, C. Shen, N. Hu, M. H. Bai, K. Zhang, Z. Tian, L. Shao, Z. Hu, X. Xu, T. Yu, K. Xie, *Nano Energy* **2020**, *78*, 105239.
- [109] Z. F. Tang, J. J. Bao, Q. X. Du, Y. Shao, M. H. Gao, B. K. Zou, C. H. Chen, *ACS Appl. Mater. Interfaces* **2016**, *8*, 34879.
- [110] Y. F. Su, Q. Y. Zhang, L. Chen, L. Y. Bao, Y. Lu, Q. Shi, J. Wang, S. Chen, F. Wu, *ACS Appl. Mater. Interfaces* **2020**, *12*, 37208.
- [111] Y. Shi, M. H. Zhang, C. C. Fang, Y. S. Meng, *J. Power Sources* **2018**, *394*, 114.
- [112] Z. Cui, Q. Xie, A. Manthiram, *ACS Appl. Mater. Interfaces* **2021**, *13*, 15324.
- [113] L. Zou, J. Li, Z. Liu, G. Wang, A. Manthiram, C. Wang, *Nat. Commun.* **2019**, *10*, 3447.
- [114] G. Qian, H. Huang, F. Hou, W. Wang, Y. Wang, J. Lin, S. J. Lee, H. Yan, Y. S. Chu, P. Pianetta, X. Huang, Z. F. Ma, L. Li, Y. Liu, *Nano Energy* **2021**, *84*, 105926.
- [115] Y. Shen, X. Yao, J. Zhang, S. Wang, D. Zhang, D. Yin, L. Wang, Y. Zhang, J. Hu, Y. Cheng, X. Li, *Nano Energy* **2022**, *94*, 106900.
- [116] Y. Kim, H. Park, K. Shin, G. Henkelman, J. H. Warner, A. Manthiram, *Adv. Energy Mater.* **2021**, *11*, 2101112.
- [117] W. Huang, W. Li, L. Wang, H. Zhu, M. Gao, H. Zhao, J. Zhao, X. Shen, X. Wang, Z. Wang, C. Qi, W. Xiao, L. Yao, J. Wang, W. Zhuang, X. Sun, *Small* **2021**, *17*, 2104282.
- [118] L. Wu, X. Tang, X. Chen, Z. Rong, W. Dang, Y. Wang, X. Li, L. Huang, Y. Zhang, *J. Power Sources* **2020**, *445*, 227337.
- [119] S. H. Park, Y. K. Sun, K. S. Park, K. S. Nahm, Y. S. Lee, M. Yoshio, *Electrochim. Acta* **2002**, *47*, 1721.
- [120] X. Li, F. Kang, W. Shen, X. Bai, *Electrochim. Acta* **2007**, *53*, 1761.
- [121] L. Fang, M. Wang, Q. Zhou, H. Xu, W. Hu, H. Li, *Colloids Surf. A* **2020**, *600*, 124940.
- [122] S. H. Song, M. Cho, I. Park, J. G. Yoo, K. T. Ko, J. Hong, J. Kim, S. K. Jung, M. Avdeev, S. Ji, S. Lee, J. Bang, H. Kim, *Adv. Energy Mater.* **2020**, *10*, 2000521.
- [123] K. Du, H. Xie, G. Hu, Z. Peng, Y. Cao, F. Yu, *ACS Appl. Mater. Interfaces* **2016**, *8*, 17713.
- [124] Y. Li, X. Liu, D. Ren, H. Hsu, G. L. Xu, J. Hou, L. Wang, X. Feng, L. Lu, W. Xu, Y. Ren, R. Li, X. He, K. Amine, M. Ouyang, *Nano Energy* **2020**, *71*, 104643.
- [125] D. Hu, Y. Su, L. Chen, N. Li, L. Bao, Y. Lu, Q. Zhang, J. Wang, S. Chen, F. Wu, *J. Energy Chem.* **2021**, *58*, 1.
- [126] K. Liu, Q. Zhang, S. Dai, W. Li, X. Liu, F. Ding, J. Zhang, *ACS Appl. Mater. Interfaces* **2018**, *10*, 34153.
- [127] H. H. Sun, J. Y. Hwang, C. S. Yoon, A. Heller, C. B. Mullins, *ACS Nano* **2018**, *12*, 12912.
- [128] Z. Chen, G.-T. Kim, D. Bresser, T. Diemant, J. Asenbauer, S. Jeong, M. Copley, R. J. Behm, J. Lin, Z. Shen, S. Passerini, *Adv. Energy Mater.* **2018**, *8*, e1801573.
- [129] J. Y. Piao, Y. G. Sun, S. Y. Duan, A. M. Cao, X. L. Wang, R. J. Xiao, X. Q. Yu, Y. Gong, L. Gu, Y. Li, Z. J. Liu, Z. Q. Peng, R. M. Qiao, W. L. Yang, X. Q. Yang, J. B. Goodenough, L. J. Wan, *Chem* **2018**, *4*, 1685.
- [130] L. Liang, X. Sun, C. Wu, L. Hou, J. Sun, X. Zhang, C. Yuan, *ACS Appl. Mater. Interfaces* **2018**, *10*, 5498.
- [131] C. W. Park, J. H. Lee, J. K. Seo, W. Y. Jo, D. Whang, S. M. Hwang, Y. J. Kim, *Nat. Commun.* **2021**, *12*, 2145.
- [132] S. Xu, C. Du, X. Xu, G. Han, P. Zuo, X. Cheng, Y. Ma, G. Yin, *Electrochim. Acta* **2017**, *248*, 534.
- [133] P. Yan, J. Zheng, J. Liu, B. Wang, X. Cheng, Y. Zhang, X. Sun, C. Wang, J. G. Zhang, *Nat. Energy* **2018**, *3*, 600.
- [134] G. Hu, Y. Tao, Y. Lu, J. Fan, L. Li, J. Xia, Y. Huang, Z. Zhang, H. Su, Y. Cao, *ChemElectroChem.* **2019**, *6*, 4773.
- [135] X. Yang, Y. Tang, Y. Qu, G. Shang, J. Wu, J. Zheng, Y. Lai, J. Li, Z. Zhang, *J. Power Sources* **2019**, *438*, 226978.
- [136] Z. Li, J. Qin, J. Liang, Z. Li, R. Wang, D. Wang, *Energy Storage Sci. Technol.* **2022**, *11*, 2900.
- [137] Y. Li, X. Li, J. Hu, W. Liu, H. Maleki Kheimeh Sari, D. Li, Q. Sun, L. Kou, Z. Tian, L. Shao, C. Zhang, J. Zhang, X. Sun, *Energy Environ. Mater.* **2020**, *3*, 522.
- [138] M. J. Herzog, D. Esken, J. Janek, *Batteries Supercaps* **2021**, *4*, 1003.
- [139] K. Du, A. Gao, L. Gao, S. Sun, X. Lu, C. Yu, S. Li, H. Zhao, Y. Bai, *Nano Energy* **2021**, *83*, 105775.
- [140] Z. Tan, Y. Li, C. Lei, Y. Li, X. Xi, S. Jiang, F. Wu, Z. He, *Small* **2023**, *20*, 2305618.
- [141] Z. Dai, J. Wang, H. Zhao, Y. Bai, *Adv. Sci.* **2022**, *9*, 2200622.
- [142] N. Phattharasupakun, J. Wuttiprom, S. Duangdangchote, S. Sarawutanukul, C. Tomon, F. Duriyasart, S. Tubtimkuna, C. Aphirakaramwong, M. Sawangphruk, *Energy Storage Mater.* **2021**, *36*, 485.
- [143] H. Yu, Y. Cao, L. Chen, Y. Hu, X. Duan, S. Dai, C. Li, H. Jiang, *Nat. Commun.* **2021**, *12*, 4564.
- [144] Y. K. Sun, S. T. Myung, M. H. Kim, J. Prakash, K. Amine, *J. Am. Chem. Soc.* **2005**, *127*, 13411.
- [145] Y. K. Sun, S. T. Myung, B. C. Park, J. Prakash, I. Belharouak, K. Amine, *Nat. Mater.* **2009**, *8*, 320.
- [146] S. J. Yoon, S. T. Myung, H. J. Noh, J. Lu, K. Amine, Y. K. Sun, *ChemSusChem* **2014**, *7*, 3295.
- [147] Z. Huang, J. Yan, Z. Liu, W. Wang, Y. Tang, Z. Zhang, T. Yang, X. Wang, X. Li, Q. Kong, S. Lan, H. Zhu, Y. Ren, Q. Liu, *Adv. Funct. Mater.* **2024**, *34*, 2400956.
- [148] Y. K. Sun, Z. Chen, H. J. Noh, D. J. Lee, H. G. Jung, Y. Ren, S. Wang, C. S. Yoon, S. T. Myung, K. Amine, *Nat. Mater.* **2012**, *11*, 942.
- [149] U. H. Kim, E. J. Lee, C. S. Yoon, S. T. Myung, Y. K. Sun, *Adv. Energy Mater.* **2016**, *6*, 1601417.
- [150] R. Lin, S.-M. Bak, Y. Shin, R. Zhang, C. Wang, K. Kisslinger, M. Ge, X. Huang, Z. Shadike, A. Pattammattel, H. Yan, Y. Chu, J. Wu, W. Yang, M. S. Whittingham, H. L. Xin, X.-Q. Yang, *Nat. Commun.* **2021**, *12*, 2021.
- [151] B. B. Lim, S. J. Yoon, K. J. Park, C. S. Yoon, S. J. Kim, J. J. Lee, Y. K. Sun, *Adv. Funct. Mater.* **2015**, *25*, 4673.
- [152] C. S. Yoon, K. J. Park, U. H. Kim, K. H. Kang, H. H. Ryu, Y. K. Sun, *Chem. Mater.* **2017**, *29*, 10436.
- [153] J. Leng, J. Wang, W. Peng, Z. Tang, S. Xu, Y. Liu, J. Wang, *Small* **2021**, *17*, 2006869.
- [154] B. Huang, M. Wang, Y. Zuo, Z. Zhao, X. Zhang, Y. Gu, *Solid State Ionics* **2020**, *345*, 115200.
- [155] H. Li, J. Li, X. Ma, J. R. Dahn, *J. Electrochim. Soc.* **2018**, *165*, A1038.
- [156] Y. Kim, *ACS Appl. Mater. Interfaces* **2012**, *4*, 2329.
- [157] J. Langdon, A. Manthiram, *Energy Storage Mater.* **2021**, *37*, 143.
- [158] X. H. Meng, T. Lin, H. Mao, J. L. Shi, H. Sheng, Y. G. Zou, M. Fan, K. Jiang, R. J. Xiao, D. Xiao, L. Gu, L. J. Wan, Y. G. Guo, *J. Am. Chem. Soc.* **2022**, *144*, 11338.
- [159] N.-Y. Park, H.-U. Lee, T.-Y. Yu, I.-S. Lee, H. Kim, S.-M. Park, H.-G. Jung, Y.-C. Jung, Y.-K. Sun, *Nat. Energy* **2025**.
- [160] C. Wang, R. Yu, S. Hwang, J. Liang, X. Li, C. Zhao, Y. Sun, J. Wang, N. Holmes, R. Li, H. Huang, S. Zhao, L. Zhang, S. Lu, D. Su, X. Sun, *Energy Storage Mater.* **2020**, *30*, 98.
- [161] Z. Dai, X. Sun, R. Chen, F. Wu, L. Li, *J. Am. Chem. Soc.* **2024**, *146*, 34517.
- [162] F. Li, Y.-C. Wu, X.-B. Cheng, Y. Tan, J.-D. Luo, R. Pan, T. Ma, L.-L. Lu, X. Wen, Z. Liang, H.-B. Yao, *Energy Environ. Sci.* **2024**, *17*, 4187.
- [163] Q. Zhou, H. Zhao, C. Fu, J. Jian, H. Huo, Y. Ma, C. Du, Y. Gao, G. Yin, P. Zuo, *Angew. Chem. Int. Ed.* **2024**, *63*, e202402625.
- [164] Y. Dai, J. Tan, Z. Hou, B. You, G. Luo, D. Deng, W. Peng, Z. Wang, H. Guo, X. Li, G. Yan, H. Duan, Y. Wang, F. Wu, J. Wang, *ACS Nano* **2024**, *18*, 22518.
- [165] Y. Orikasa, K. Yamamoto, T. Shimizu, Y. Uchimoto, *Chem. Phys. Rev.* **2022**, *3*, 011305.
- [166] S. Lee, A. Manthiram, *ACS Energy Lett.* **2022**, *7*, 3058.
- [167] F. Zhang, S. Lou, S. Li, Z. Yu, Q. Liu, A. Dai, C. Cao, M. F. Toney, M. Ge, X. Xiao, W.-K. Lee, Y. Yao, J. Deng, T. Liu, Y. Tang, G. Yin, J. Lu, D. Su, J. Wang, *Nat. Commun.* **2020**, *11*, 3050.

Manuscript received: February 13, 2025

Revised manuscript received: April 7, 2025

Version of record online: April 10, 2025